



PhoU2 but Not PhoU1 as an Important Regulator of Biofilm Formation and Tolerance to Multiple Stresses by Participating in Various Fundamental Metabolic Processes in *Staphylococcus epidermidis*

Xiaofei Wang,^a Haiyan Han,^{a,d} Zhihui Lv,^a Zhiwei Lin,^a Yongpeng Shang,^a Tao Xu,^b Yang Wu,^a Ying Zhang,^{b,c} Di Qu^a

Department of Medical Microbiology and Parasitology, Key Laboratory of Medical Molecular Virology of MOE and MOH, School of Basic Medical Sciences, Fudan University, Shanghai, China^a; Key Laboratory of Medical Molecular Virology, Huashan Hospital, Shanghai Medical College of Fudan University, Shanghai, China^b; Department of Molecular Microbiology and Immunology, Bloomberg School of Public Health, Johns Hopkins University, Baltimore, Maryland, USA^c; Department of Laboratory Medicine in the Second Affiliated Hospital of Zhengzhou University, Zhengzhou, China^d

ABSTRACT PhoU, a conserved protein that has been proposed to coordinate phosphate import, is a negative regulator of drug tolerance in most bacteria. In *Staphylococcus epidermidis*, the role of PhoU in biofilm formation and drug tolerance has not yet been investigated. Two PhoU homologs in the genome of *S. epidermidis* have been identified by the presence of the conserved motif E(D)XXXD of PhoU. We separately constructed $\Delta phoU1$ and $\Delta phoU2$ mutants of *S. epidermidis* strain 1457. The $\Delta phoU2$ mutant displayed growth retardation, a weakened biofilm formation capacity, a higher sensitivity to H₂O₂, and reduced tolerance to multiple antibiotics. However, deletion of *phoU1* had no effect on those. We compared the transcriptome profiles of the $\Delta phoU2$ and $\Delta phoU1$ mutants with that of the parent strain. In the $\Delta phoU2$ mutant, expression of genes related to inorganic phosphate uptake was significantly upregulated (*pst* operon) and the levels of intracellular inorganic polyphosphate (polyP) were increased. In the $\Delta phoU2$ mutant, expression of enzymes in the pentose phosphate pathway (PPP) was downregulated and less NADP (NADPH) was detected, consistent with the high sensitivity to H₂O₂ and the growth retardation of the $\Delta phoU2$ mutant. The upregulated expression of ATP synthase was consistent with the high intracellular ATP content in the $\Delta phoU2$ mutant, which may have been related to the lower drug tolerance of the $\Delta phoU2$ mutant. This study demonstrates that PhoU2, but not PhoU1, in *S. epidermidis* regulates bacterial growth, biofilm formation, oxidative stress, and drug tolerance in association with alterations to inorganic phosphate metabolism, the pentose phosphate pathway, galactose metabolism, the tricarboxylic acid (TCA) or citric cycle, glycolysis and gluconeogenesis, and respiratory reactions.

IMPORTANCE PhoU is widely conserved throughout the bacterial kingdom and plays an important role in response to stress and metabolic maintenance. In our study, two PhoU homologs were found in *S. epidermidis*. The function of *phoU2*, but not *phoU1*, in *S. epidermidis* is related to growth, drug tolerance, the oxidative stress response, polyP levels, and ATP accumulation. In addition, *phoU2* regulates biofilm formation. Hence, *phoU2* is a regulator of both drug tolerance and biofilm formation, which are two bacterial properties that present major challenges to the clinical treatment of infections. Analysis of differential gene expression revealed that *phoU2* is in-

Received 23 March 2017 Accepted 18 August 2017

Accepted manuscript posted online 25 September 2017

Citation Wang X, Han H, Lv Z, Lin Z, Shang Y, Xu T, Wu Y, Zhang Y, Qu D. 2017. PhoU2 but not PhoU1 as an important regulator of biofilm formation and tolerance to multiple stresses by participating in various fundamental metabolic processes in *Staphylococcus epidermidis*. *J Bacteriol* 199:e00219-17. <https://doi.org/10.1128/JB.00219-17>.

Editor Victor J. DiRita, Michigan State University

Copyright © 2017 Wang et al. This is an open-access article distributed under the terms of the [Creative Commons Attribution 4.0 International license](https://creativecommons.org/licenses/by/4.0/).

Address correspondence to Ying Zhang, yzhang@jhsph.edu, or Di Qu, dqu@shmu.edu.cn. X.W. and H.H. contributed equally to this article.

volved in fundamental metabolic processes, such as the PPP pathway. These findings indicate that *phoU2* is a crucial regulator in *S. epidermidis*.

KEYWORDS biofilm, *Staphylococcus epidermidis*, tolerance

Staphylococcus epidermidis is a common opportunistic pathogen that is present on human skin and mucosal surfaces. The pathogenicity of *S. epidermidis* is mainly due to biofilm formation on foreign devices, such as catheters, heart valves, and prostheses (1, 2). The bacteria within the biofilm are protected against killing by antibiotics and the host immune system, contributing to the increasing emergence of resistance to antimicrobial drugs and to the establishment of persistent infections (3, 4). PhoU, the phosphate transport system regulatory protein, is now known to be a negative regulator of drug tolerance in *Escherichia coli*, *Mycobacterium tuberculosis*, and *Pseudomonas aeruginosa* (5–8), whereas the possible role of PhoU in biofilm formation and drug tolerance in *S. epidermidis* has not been investigated.

On the basis of a crystal structure analysis of PhoU in *Thermotoga maritima* (9), multinuclear iron clusters [E(D)XXXD] have been identified to be the conserved motif of the protein. According to the conserved motif, one homolog of *phoU* is found in *E. coli*, *P. aeruginosa*, and *Streptococcus*, while two *phoU* homologs are found in *T. maritima*, *M. tuberculosis*, *Mycobacterium marinum*, and *Staphylococcus aureus*. In *E. coli* and *P. aeruginosa*, *phoU* is located in the *pst* operon, which contains four other genes: *pstS*, *pstA*, *pstC*, and *pstB*. PstS is a periplasmic inorganic phosphate (P_i)-binding protein that captures and transfers P_i to the channel formed by the integral proteins PstC and PstA in the cytoplasmic membrane. PstB is an ATPase that provides the energy for transport (10). The last gene in the operon, *phoU*, encodes a protein that does not have a defined function. In 2007, it was reported that *phoU* in *E. coli* plays an important role in the development of multidrug-tolerant bacteria (5). In *P. aeruginosa*, *phoU* is a negative regulator of intracellular ppGpp and polyphosphate (polyP), but it does not regulate biofilm formation (8). In *M. tuberculosis* and *M. marinum*, there are two *phoU* homologs in the genome, *phoY1* and *phoY2*. However, neither *phoY1* nor *phoY2* is located in the *pst* operon. In the two mycobacterial species, *phoY2* was shown to be a functional homolog of *phoU*, regulating the generation of multidrug-tolerant bacteria and maintaining metabolic homeostasis and adaptation to stress conditions (6, 7). In the *S. aureus* (NCTC8325) genome, there are two *phoU* homologs (*SAOUHSC_01384* and *SAOUHSC_00669*). In *S. aureus*, *SAOUHSC_01384* resides in the *pst* operon as *phoU*, while *SAOUHSC_00669* (*pitR*) also contains the conserved motif of *phoU* and is located upstream of *pitA* (a phosphate uptake gene). A point mutation in *pitA* in *S. aureus* resulted in bacteria that were sensitized to daptomycin, and *SAOUHSC_00669* was found to be required for daptomycin sensitivity (11, 12). In the present study, protein motif analysis of *S. epidermidis* ATCC 35984 revealed two genes that were homologous to *phoU* (*serp0956* and *serp0316*). *serp0956*, found in the *pst* operon, was named *phoU1*, while *serp0316*, located upstream of a hypothetical protein with a high degree of homology to *pitR* of *S. aureus*, was named *phoU2*.

In staphylococci, biofilm formation and drug tolerance are regulated by multiple regulatory factors (13, 14). In this study, we focused on investigating the roles of PhoU homologs in the biofilm formation and drug tolerance of *S. epidermidis*. In *S. epidermidis* strain 1457 (SE1457), either *phoU1* or *phoU2* was deleted by allelic replacement to create the Δ *phoU1* and Δ *phoU2* mutants, respectively. The effects of these deletions on bacterial growth, biofilm formation, drug tolerance, and oxidative stress were investigated. Comparison of the transcriptomes of the Δ *phoU2* mutant and the parent strain revealed the differentially expressed genes (DEGs) involved in the pentose phosphate (PPP) pathway, galactose metabolism, the trichloroacetic acid (TCA) cycle, glycolysis and gluconeogenesis, and respiratory chain reactions. The involvement of some of the DEGs in metabolic processes, such as polyP accumulation, ATP accumulation, and the pentose phosphate pathway, was validated. We conclude that *phoU2* probably regulates bacterial growth, biofilm formation, oxidative stress responses, and drug tolerance

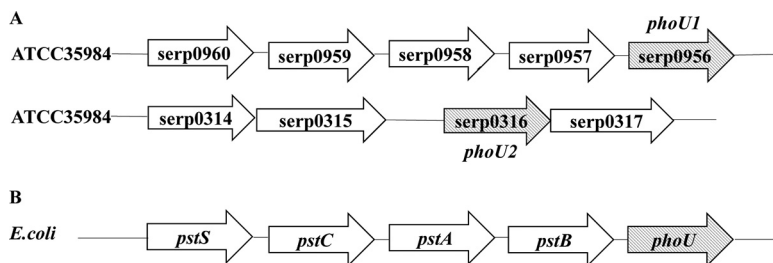


FIG 1 Two genes homologous to *phoU*, *phoU1* and *phoU2*, were found in *S. epidermidis* RP62A by motif analysis according to the PhoU conserved motifs [E(D)XXXD] of *Thermotoga maritima*. (A) Genetic locations of *phoU1* and *phoU2* in *S. epidermidis* RP62A. (B) Genetic organization of the *pst* operon and *phoU* in *E. coli*.

in *S. epidermidis*. In contrast, *phoU1* has no obvious effect on biological activity in *S. epidermidis*.

RESULTS

The two *phoU* loci identified in the genome of *S. epidermidis*. In the genome of the *S. epidermidis* ATCC 35984 strain (GenBank accession number CP000029), two PhoU gene homologs, *serp0956* and *serp0316*, were identified by bioinformatics analysis (<https://www.ncbi.nlm.nih.gov/genome/?term=RP62a>) on the basis of the conserved motif E(D)XXXD of *Thermotoga maritima*. *serp0956* is located in the *pst* operon, similarly to the *phoU* gene in *E. coli*, which is denoted as encoding a phosphate transport system regulatory protein and designated *phoU1* in this study. *serp0316*, denoted *phoU2*, encodes a hypothetical protein, is located far from the *pst* operon, and was cotranscribed with the adjacent gene, *serp0317* (Fig. 1). The two PhoU homologs in *S. epidermidis* shared 12.5% identity and 30.1% consensus sequences.

Construction of *phoU1* and *phoU2* deletion strains. To identify the function of *phoU1* or *phoU2* in *S. epidermidis*, mutants of the SE1457 strain with a deletion of *phoU1* or *phoU2* were constructed using the temperature-sensitive plasmid pKOR1. The deletion mutants were verified by PCR, reverse transcription (RT)-quantitative PCT (qPCR), and direct sequencing and are referred to as the $\Delta phoU1$ and $\Delta phoU2$ mutants, respectively. The complemented $\Delta phoU2$ strain was constructed using shuttle vector pCN51 and named SE1457 $\Delta phoU2$ /pCN51::*phoU2*. The $\Delta phoU2$ strain containing the empty vector pCN51 was designated SE1457 $\Delta phoU2$ /pCN51.

Growth curves of the $\Delta phoU1$ and $\Delta phoU2$ mutants. To evaluate the effect of *phoU1* or *phoU2* knockout on the growth of *S. epidermidis*, growth curves of the $\Delta phoU1$ and $\Delta phoU2$ mutants and the parent strain (SE1457) were generated under oxic and microaerobic conditions.

Under oxic conditions, in comparison to the parent strain, the $\Delta phoU2$ mutant displayed a marked reduction in growth (Fig. 2A). However, the $\Delta phoU1$ mutant displayed growth curves and colony sizes similar to those of the parent strain when the strains were incubated under the same conditions. By culture in liquid tryptic soya broth (TSB) medium at 37°C for 6 h, the optical density at 600 nm (OD_{600}) of the $\Delta phoU2$ mutant reached 1.26 ± 0.343 , and that of the parent strain was 2.41 ± 0.078 . On solid culture medium (TSB agar), the colony size of the $\Delta phoU2$ mutant was much smaller than that of the parent strain (Fig. 2C). The expression of *phoU2* by the pCN51 vector restored the growth of the $\Delta phoU2$ mutant to the level of the parent strain.

Under microaerobic conditions, the growth rates of the $\Delta phoU1$ and $\Delta phoU2$ mutants and SE1457 in liquid medium were measured by recording the OD_{600} of the cultures. After 6 h of incubation, the OD_{600} of the $\Delta phoU2$ mutant was 0.265 ± 0.04 , which was much less than that of SE1457 (0.418 ± 0.03) (Fig. 2B). However, no differences in the growth curve could be detected in the $\Delta phoU1$ mutant when the strains were incubated under the same conditions.

Morphology and autolysis of the $\Delta phoU1$ and $\Delta phoU2$ mutants. The morphologies of the $\Delta phoU1$ and $\Delta phoU2$ mutants and the parent strain were observed using

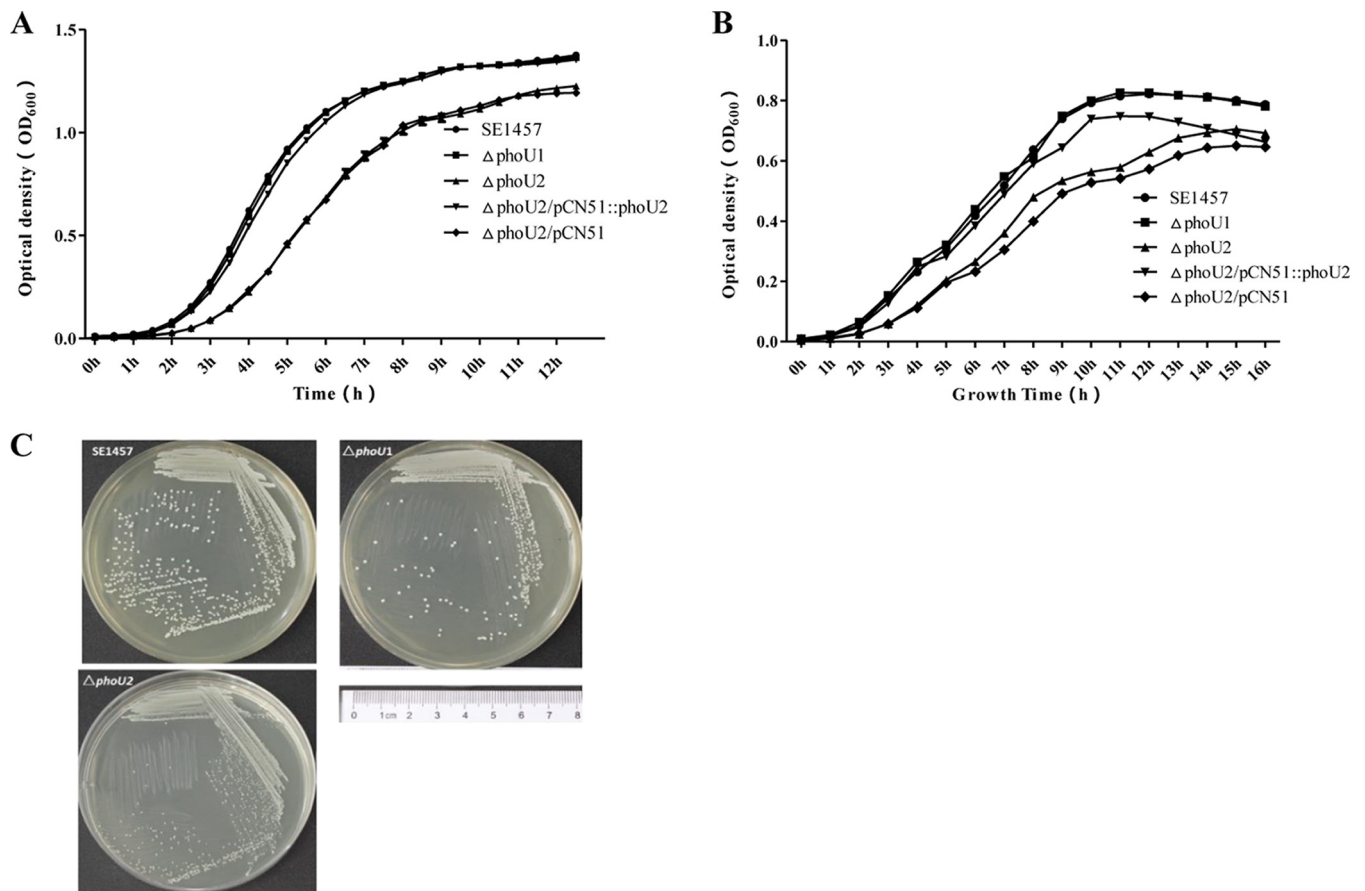


FIG 2 Effect of *phoU2* deletion on the growth of *S. epidermidis*. Overnight cultures of the $\Delta phoU1$, $\Delta phoU2$, and SE1457 strains were diluted 1:200 into 10 ml TSB in a conical flask in a volume of 100 ml and incubated with shaking at 220 rpm. Bacterial growth was monitored by measuring the OD_{600} for 12 h. Data (means \pm SDs) are from three independent experiments. (A) Growth curves of the $\Delta phoU1$ and $\Delta phoU2$ mutants under oxic conditions. (B) Growth curves of $\Delta phoU1$ and $\Delta phoU2$ mutants under microaerobic conditions. (C) Representative images showing the colony morphology of the $\Delta phoU1$ and $\Delta phoU2$ mutants and the SE1457 parent strain grown on TSB agar plates at 37°C for 24 h under oxic conditions. The results represent those from one of three independent experiments.

transmission electron microscopy (TEM). A rough cell wall and thin cytoplasm were observed in the $\Delta phoU2$ mutant (magnification, $\times 26,500$), while the morphology of the $\Delta phoU1$ mutant was similar to that of the parent strain (Fig. 3A).

The autolysis capacity of the $\Delta phoU1$ and $\Delta phoU2$ mutants and the parent strain was then assessed by Triton X-100 induction. Mid-exponential-phase cultures (6 h) of the $\Delta phoU1$ and $\Delta phoU2$ mutants and SE1457 were adjusted to an OD_{600} of 1.0 and incubated with 0.05% Triton X-100 for 5 h, and the autolysis rate was measured by determination of the OD_{600} using a spectrophotometer. After Triton X-100 induction, the autolysis rate of the $\Delta phoU2$ mutant reached 88% after treatment for 3 h, which was significantly higher than that of SE1457 (46%). The autolysis rate of $\Delta phoU1$ (43%) was similar to that of the parent strain (Fig. 3B).

Biofilm formation of the $\Delta phoU1$ and $\Delta phoU2$ mutants under static or hydrodynamic conditions. Under static conditions, the polystyrene microtiter plate assay and the confocal laser scanning microscopy (CLSM) observation assay were performed to evaluate the role of *phoU1* or *phoU2* in biofilm formation. Bacterial biofilm formation was monitored at 6, 12, 24, and 48 h on microtiter plates stained with crystal violet, and the OD_{570} was read. The mature biofilm of the $\Delta phoU2$ mutant (OD_{570} , 1.56 ± 0.10) was significantly decreased compared with that of the parent strain (OD_{570} , 3.04 ± 0.08) after incubation for 24 h, and the $\Delta phoU1$ deletion (OD_{570} , 2.58 ± 0.02) had little effect on biofilm formation (Fig. 4). The complemented $\Delta phoU2/pCN51::phoU2$ strain (OD_{570} , 2.77 ± 0.12) showed a restored biofilm formation ability.

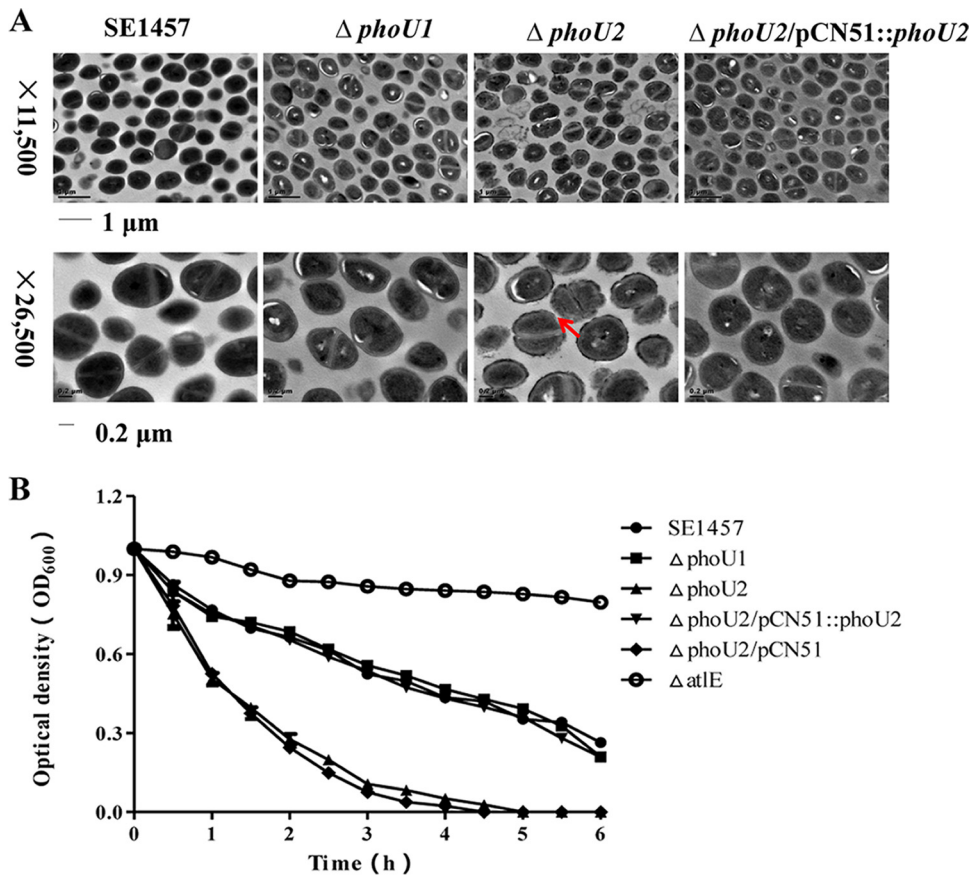


FIG 3 (A) Bacterial morphology of the $\Delta phoU1$ and $\Delta phoU2$ mutants observed by TEM. The ultrastructure of the log-phase bacteria was observed by transmission electron microscopy (Phillips Tecnai-12 Biotwin). Arrow, disruption of the cell wall in the $\Delta phoU2$ mutant. (B) Autolysis of the $\Delta phoU1$ and $\Delta phoU2$ mutants induced by Triton X-100. Overnight cultures were suspended in Triton X-100 autolysis buffer (50 mM glycine, pH 8.0, containing 0.01% Triton X-100) to an initial OD₆₀₀ of approximately 1.0, and the rates of autolysis were monitored on the basis of the decrease in the OD₆₀₀ value over time.

Furthermore, the biofilm formation ability of the $\Delta phoU2$ mutant *in vitro* was examined by confocal laser scanning microscopy. After incubation at 37°C for 24 h, SE1457 formed a compact, thick biofilm on a glass coverslip in a cell culture dish. In contrast, the biofilm of the $\Delta phoU2$ mutant was much thinner than that of the parent

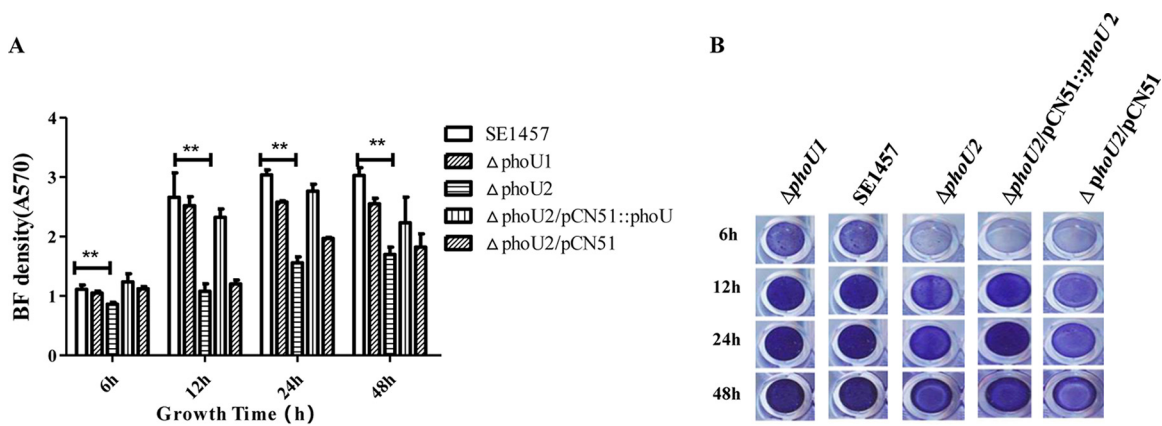


FIG 4 Biofilm (BF) formation by the $\Delta phoU1$ and $\Delta phoU2$ mutants on microtiter plates. Overnight cultures of the *S. epidermidis* strains were diluted 1:200 with fresh TSB, added to 96-well polystyrene plates in triplicate, and cultured under static conditions for 6 h, 12 h, 24 h, and 48 h. After the biofilms were washed, they were stained with crystal violet. The OD₅₇₀s of the plates were analyzed. The experiments were repeated three times, and the data represent means \pm SDs. **, $P < 0.01$.

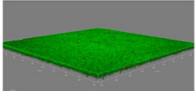
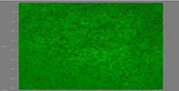
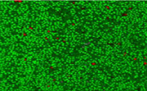
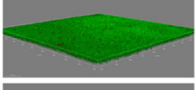
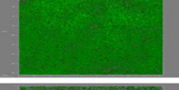
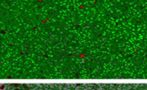
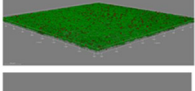

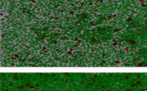
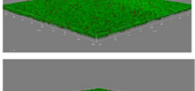

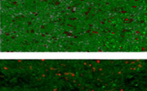
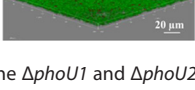

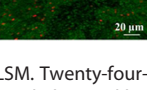
	3-D structure	Middle layer	Merged Z-series	Thickness (μm)	SYTO9	PI	PI/Total
SE1457				20.6	121.7	1.6	1.3%
ΔphoU1				21.4	149.8	1.9	1.3%
ΔphoU2				12.3	100.8	7.3	6.7%
$\Delta\text{phoU2}/\text{pCN51}::\text{phoU2}$				19.5	111.9	3.1	2.7%
$\Delta\text{phoU2}/\text{pCN51}$				13.7	102.3	7.7	7.0%

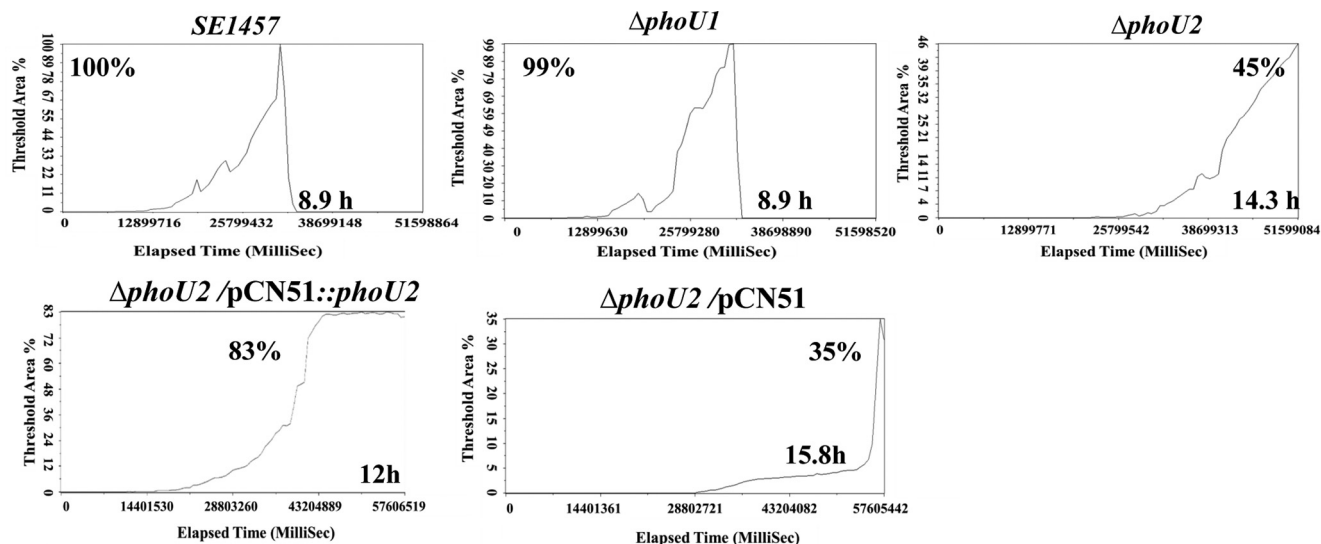
FIG 5 Biofilms of the ΔphoU1 and ΔphoU2 mutants observed by CLSM. Twenty-four-hour-old biofilms of SE1457 and the ΔphoU1 and ΔphoU2 mutants were grown on a cover glass in a cell culture dish and observed by CLSM. Three-dimensional (3-D) structural images (zoom 1, $\times 63$ magnification) were reconstructed, and the thickness of the biofilms was measured using Imaris software. Viable and dead cells were stained green (SYTO9) and red (PI), respectively. The amount of fluorescence in the middle layer of the biofilm was determined using ImageJ software (zoom 3, $\times 63$ magnification). The PI/total fluorescence value indicates the proportion of dead cells within the biofilm. The images and values are representative of those from one of three independent experiments.

strain. Additionally, the dead cell ratio in the biofilm of the ΔphoU2 mutant (6.7%) was 5-fold higher than that in the biofilm of the parent strain (1.3%) (Fig. 5).

Under hydrodynamic conditions, the biofilm formation of the ΔphoU2 mutant strain was analyzed using a BioFlux 1000 device with a flow speed of 0.15 dyne/cm^2 . The maximum size of the biofilm of the ΔphoU2 mutant observed in the channel was 2-fold smaller than that of the biofilm of the parent strain and the complemented strain, and the time required to form the maximum biofilm was 5.4 h longer for the ΔphoU2 mutant strain than for the parent strain (Fig. 6). The biofilm formation of the ΔphoU1 mutant in the hydrodynamic state appeared to be similar to that of the parent strain. The complemented $\Delta\text{phoU2}/\text{pCN51}::\text{phoU2}$ strain could partially restore the biofilm formation capacity under hydrodynamic conditions.

The initial attachment phase is characterized as the first phase of the process of *Staphylococcus epidermidis* biofilm formation. The initial attachment capacity of the ΔphoU2 mutant was determined, and the attached cells were counted using ImageJ software. There were fewer attached cells for the ΔphoU2 mutant (3.32×10^6) than for the parent strain (2.70×10^7) and the complemented strain $\Delta\text{phoU2}/\text{pCN51}::\text{phoU2}$ (2.33×10^7). The number of attached cells of the ΔphoU1 mutant (2.47×10^7) was similar to the number of attached cells of the parent strain (Fig. 7).

To investigate the effect of the *phoU2* deletion on biofilm matrix production, the release of accumulation-associated protein (Aap), polysaccharide intercellular adhesion (PIA), and extracellular DNA (eDNA) was determined for SE1457 and the ΔphoU1 and ΔphoU2 mutants. The production of Aap was reduced in the biofilm of the ΔphoU2 mutant compared with that in the biofilm of the parent strain (Fig. 8A), as determined by Western blotting with monoclonal antibody 18B6 (MAb_{18B6}) against the Aap protein B repeat region. PIA production was similar in the ΔphoU2 mutant biofilm and the parent strain, as determined semiquantitatively with a wheat germ agglutinin (WGA)-horseradish peroxidase (HRP) conjugate using a dot blot 96 system (Fig. 8B). The relative concentration of eDNA in the 24-h-old biofilm of the ΔphoU2 mutant was similar to that in the parent strain (Fig. 8C). All *P* values were >0.05 , so there were no differences in the levels of transcription of *serp0306*, *leuA*, or *lysA* between biofilm bacteria of the PhoU mutants and the parent strain. The levels of PIA, Aap, and eDNA production were similar in the ΔphoU1 mutant and the parent strain.



Strain	Maximum Biofilm production	Reaching time
SE1457	100%	8.9 h
<i>ΔphoU1</i>	99%	8.9 h
<i>ΔphoU2</i>	45%	14.3 h
<i>ΔphoU2/pCN51</i>	83%	12 h
<i>ΔphoU2/pCN51::phoU2</i>	35%	15.8 h

FIG 6 Biofilm formation by the *ΔphoU1* and *ΔphoU2* mutants under hydrodynamic conditions. Overnight cultures of the *S. epidermidis* strains were diluted 1:200 with fresh TSB and added to BioFlux 48-well plates. The bacteria were then cultured under hydrodynamic conditions with a shear setting of 0.15 dyne/cm². A BioFlux 1000 system (Fluxion Biosciences) with a Leica microscope and temperature-controlled housing was used for all imaging experiments. Automated microscopy and image processing were performed with BioFlux Montage software. Images were automatically acquired every 10 min at multiple stage positions with bright-field illumination; images were also acquired in the red channel using a 200-ms exposure time. The background-corrected average pixel intensity per image was used to quantify the biofilm formation by the different strains. The curve was generated on the basis of the images. A synthesis of the images is shown in Movies S1 to S5 in the supplemental material. Each figure represents the results of one of three independent experiments.

Antibiotic tolerance of the *ΔphoU1* and *ΔphoU2* mutants. Antibiotic-tolerant bacteria were identified using a modification of a procedure described by Li and Zhang (5). Both the MIC and the minimal bactericidal concentration (MBC) for the *ΔphoU1* and *ΔphoU2* mutants were similar to those for the parent strain. To determine the antibiotic concentrations that ensured that only drug-tolerant bacterial cells survived, killing curves were determined for each antibiotic used in the present study. To detect the drug tolerance of the bacterial mutants, in which the size of the population of bacteria was not decreased with an increase in the antibiotic concentration, the concentrations of antibiotics were as follows: vancomycin, 75 μg/ml (96× MIC); levofloxacin, 75 μg/ml (128× MIC); amikacin, 50 μg/ml (128× MIC).

An overnight culture (16 h) of *S. epidermidis* was inoculated into fresh TSB (at 1:100) containing the antibiotics at the specific concentrations, and the culture was incubated at 37°C for 5 days. At different time points, the surviving bacteria were counted. After exposure to the three antibiotics for 72 h, the antibiotic tolerance of the *ΔphoU2* mutant was dramatically reduced, and no viable bacteria were detected. In contrast, the *ΔphoU1* mutant displayed an antibiotic tolerance similar to that of the parent strain (greater than 10⁴ CFU) (Table 1). The complementation of the *ΔphoU2* mutant strain restored the antibiotic tolerance.

Comparison of the transcriptomes of the *ΔphoU2* mutant and the parent strain. To compare the transcriptional profile of the *ΔphoU1* or *ΔphoU2* mutant with that of SE1457, RNA was extracted from logarithmic-phase (6 h) and stationary-phase (10 h) bacteria and detected by transcriptome sequencing (RNA-Seq). The sequencing

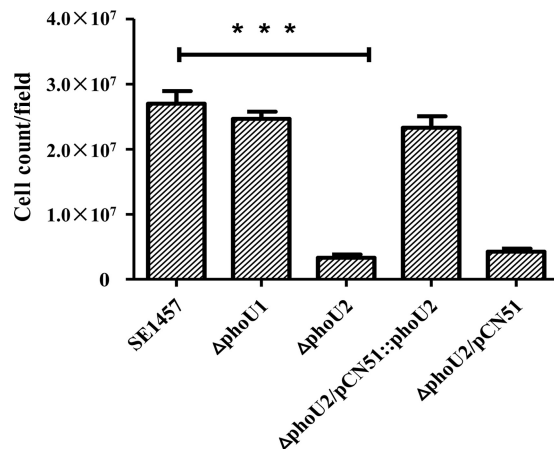


FIG 7 Initial attachment of the $\Delta phoU1$ and $\Delta phoU2$ mutants on polystyrene plates. Log-phase bacterial cultures in TSB were adjusted to an OD_{600} of 0.1 with PBS, and 5-ml aliquots were added to a 6-well polystyrene plate. After incubation at 37°C for 30 min, each well was washed three times with PBS, and the adhered cells were observed and photographed. The amounts of attached bacterial cells of the $\Delta phoU1$ and $\Delta phoU2$ mutants and SE1457 are indicated. The results (means \pm SDs) are from three independent experiments. ***, $P < 0.001$.

libraries were prepared in triplicate for the $\Delta phoU1$ and $\Delta phoU2$ mutants and the parent strain. For each biological replicate, 10 million raw reads were generated. After the removal of ambiguous and low-quality reads, more than 90% of the reads mapped to strain ATCC 35984.

A gene with a false discovery rate (FDR)-adjusted P value of less than 0.05 (t test), a q value of less than 0.05, and at least a 1.5-fold change in the transcript level between the mutant and the parent strain was considered to be differentially expressed. In logarithmic phase (6 h), 945 genes were identified to be differentially expressed between the $\Delta phoU2$ mutant and the parent strain; among these, 474 genes were upregulated and 471 were downregulated. In the stationary phase (10 h), 995 DEGs

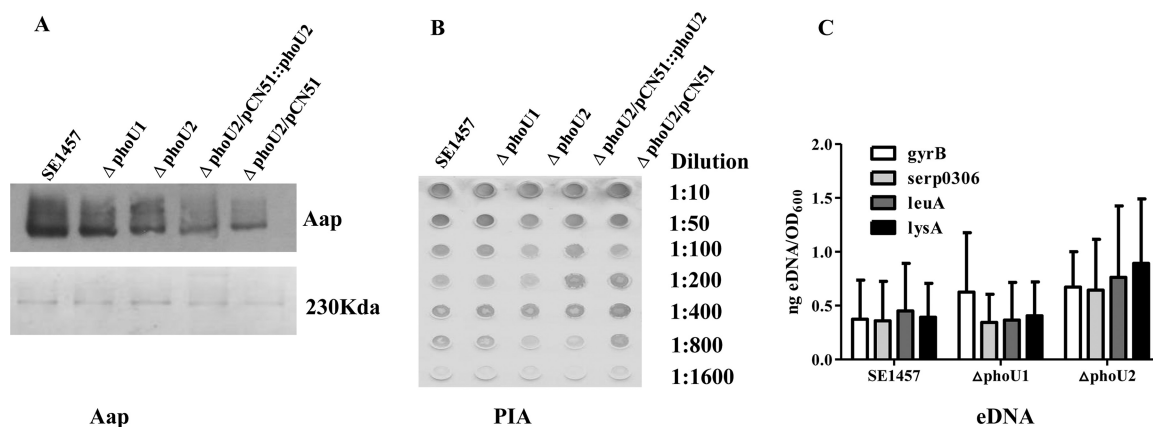


FIG 8 Effects of the $\Delta phoU1$ and $\Delta phoU2$ mutants on extracellular matrix biosynthesis by *S. epidermidis*. (A) Aap expression in the $\Delta phoU1$ and $\Delta phoU2$ mutants. Twenty-four-hour-old biofilms and 12-h-old planktonic bacteria were collected after they were washed with PBS. Lysostaphin-treated samples with identical OD_{600} s were centrifuged at $20,000 \times g$ for 30 min at 4°C. The supernatant was separated by 7% SDS-PAGE, and the gel pieces containing Aaps were used for Western blotting (top). The remaining gel pieces were stained with Coomassie blue as an endogenous reference (bottom). MAb_{18B6} (10 ng/ml) was used as the primary antibody. Immunoreactivity was detected using an ECL Western blotting system after incubation with HRP-conjugated secondary antibody. (B) PIA biosynthesis was semiquantified using a dot blot assay with WGA. Twenty-four-hour-old biofilms were scraped off and suspended in EDTA. Serial dilutions of the PIA assay extracts were spotted onto nitrocellulose membranes, subsequently incubated with WGA conjugated to HRP, and visualized by chromogenic detection. (C) eDNA quantified by qPCR of four chromosomal loci (*gyrB*, *serp0306*, *leuA*, and *lysA*). The OD_{600} s of unwashed 24-h-old biofilms were measured for normalization to the biofilm biomass, and then the biofilms were used for eDNA isolation by phenol-chloroform-isoamyl alcohol extraction and ethanol precipitation. The results are presented as the amount of eDNA per biofilm biomass (means \pm SDs) from three independent experiments.

TABLE 1 Survival of the $\Delta phoU1$ and $\Delta phoU2$ mutants and the parent strain with antibiotic exposure over time^a

Time point	No. of CFU/ml															
	$\Delta phoU1$ mutant				$\Delta phoU2$ mutant				$\Delta phoU2/pCN51::phoU2$ strain				$\Delta phoU2/pCN51$ strain			
	Van	Lev	Ami	Van	Lev	Ami	Van	Lev	Ami	Van	Lev	Ami	Van	Lev	Ami	
Start	8×10^9	8×10^9	8×10^9	8.7×10^9	8.7×10^9	8.7×10^9	9×10^9	9×10^9	9×10^9	8.5×10^9	8.5×10^9	8.5×10^9	8.7×10^9	8.7×10^9	8.7×10^9	
12 h	6×10^6	4×10^6	7.2×10^6	8×10^6	7.8×10^6	4.4×10^6	8×10^5	5×10^4	6×10^5	6.8×10^6	5×10^6	7.8×10^6	7.6×10^6	5.7×10^4	4×10^5	
24 h	3.2×10^6	3.6×10^6	5×10^5	6×10^6	5×10^6	4×10^6	5×10^5	2×10^3	1×10^5	4×10^6	3.5×10^6	2×10^6	3.5×10^5	5×10^3	2.4×10^4	
36 h	9.2×10^5	7×10^5	4×10^5	1.2×10^6	2.4×10^6	2×10^6	5.4×10^5	0	6×10^4	2.2×10^6	8×10^5	7×10^5	4×10^4	0	2×10^3	
48 h	1.3×10^6	5×10^5	8.8×10^4	1.28×10^6	3×10^6	5×10^5	4×10^4	0	1.2×10^4	7×10^5	8×10^5	4.5×10^5	2.4×10^3	0	0	
72 h	4.4×10^6	2×10^5	6×10^4	2.57×10^6	5×10^5	4×10^5	0	0	0	5×10^5	4.6×10^5	9×10^4	0	0	0	
96 h	6×10^6	7×10^5	4×10^4	9×10^6	6.6×10^5	1×10^5	0	0	0	7.2×10^5	5×10^5	7.5×10^4	0	0	0	
120 h	1.9×10^5	6×10^5	1.9×10^4	6×10^6	4×10^5	8×10^4	0	0	0	2.4×10^5	4.5×10^5	5×10^4	0	0	0	

^aThe susceptibilities of stationary-phase cultures of the $\Delta phoU1$ and $\Delta phoU2$ mutants and the SE1457 parent strain to vancomycin (Van; 75 $\mu\text{g/ml}$), levofloxacin (Lev; 75 $\mu\text{g/ml}$), and amikacin (Ami; 50 $\mu\text{g/ml}$) were determined. The numbers of CFU were determined at different times of exposure of stationary-phase cultures of these strains to the indicated antibiotics.

were identified; among these, 716 genes were upregulated and 279 were downregulated. By comparison and analysis, 439 DEGs were identified in the different phases of both the $\Delta phoU2$ mutant and the parent strain. Among these genes, 256 showed the same expression tendency. However, there were only 92 genes differentially expressed between the $\Delta phoU1$ mutant and the parent strain during logarithmic phase and 2 DEGs during the stationary phase. Therefore, we focused on analyzing the genes differentially expressed between the $\Delta phoU2$ mutant and the parent strain. We selected 70 of the DEGs for validation by RT-qPCR. Among them, the transcription of 62 genes in the $\Delta phoU2$ mutant was consistent with the tendency observed by RNA-Seq. The other 8 genes determined by RT-qPCR displayed a fold change in expression below the cutoff value of 2.

Among the DEGs, the transcription of *yycFG*, an essential two-component system for regulating bacterial growth, in the $\Delta phoU2$ mutant was downregulated 3-fold compared with its expression in the parent strain (15). Transcription of the anaerobic growth-regulated genes *pflA*, *nrdD*, and *nrdG* was downregulated in the $\Delta phoU2$ mutant (16–19). The expression of *rsbU* (a sigma factor B regulatory protein), which is involved in biofilm formation, was also downregulated (20). Transcription of the autolysis genes *ssaA* (*serp2136*, *serp1880*, *serp1884*, *serp2120*) and *serp0318* was upregulated in the $\Delta phoU2$ mutant, while the gene for autolysin E (*atlE*) was not found among the DEGs (21–23). Expression of the *pst* operon and *phoR*, involved in inorganic phosphate metabolism, was upregulated in the $\Delta phoU2$ mutant, while that of the *phn* ABC transporter, which participates in phosphonate metabolism, was downregulated. The expression of ATP synthase was upregulated (Table 2).

Using KEGG analysis, the genes differentially expressed between the $\Delta phoU2$ mutant and the parent strain were involved not only in phosphate metabolism, bacterial growth, and biofilm formation but also in various pathways or processes, such as the pentose phosphate pathway, galactose metabolism, the TCA cycle, glycolysis and gluconeogenesis, respiratory chain reactions, ABC transporter activity, the phosphotransferase (PTS) system, the urea cycle, and ribosome protein production (Table 2).

To further determine the links between the DEGs and the biological behavior in the $\Delta phoU2$ mutant, a protein-protein interaction (PPI) network of DEGs based on the KEGG database (<http://www.genome.jp/kegg/pathway.html>) was constructed using Cytoscape software. The proteins encoded by DEGs were pooled with 174 proteins involved in various metabolic pathways. The expression of genes for proteins involved in the pentose phosphate pathway, galactose metabolism, and amino acid synthesis and TCA cycle genes was downregulated (Fig. 9). In the pentose phosphate pathway, NADP (NADPH) and pentose are important products. NADPH plays a crucial role in coping with oxidative stress (24–29). As pentose is utilized to synthesize DNA and RNA, the absence of DNA and RNA in the $\Delta phoU2$ mutant leads to bacterial growth retardation.

Biological validation of genes differentially expressed between the $\Delta phoU2$ mutant and the parent strain. DEGs related to inorganic phosphate metabolism, ATP synthesis, and the pentose phosphate pathway were validated by the detection of intracellular polyP, ATP, and NADPH, respectively.

The expression of DEGs involved in inorganic phosphate metabolism, the *pst* operon, and *serp0317* was upregulated in the $\Delta phoU2$ mutant. Inorganic phosphate (P_i) taken up from the environment is used in bacterial metabolism, and the redundant inorganic phosphate is stored as a high-molecular-weight inorganic polyphosphate (polyP) in bacterial cells. To investigate the effects of the $\Delta phoU1$ and $\Delta phoU2$ deletions on P_i removal, we evaluated the levels of intracellular polyP in bacterial cells using a DAPI (4',6-diamidino-2-phenylindole)-based fluorescence approach. The results showed that $\Delta phoU2$ mutant cells accumulated higher levels of polyP (1.66-fold) than the parent strain ($P < 0.05$), while the amount of intracellular polyP in the $\Delta phoU1$ mutant was similar to that in the parent strain (Fig. 10A). The polyP content in the *phoU2*-complemented $\Delta phoU2/pCN51::phoU2$ strain was restored to that in the parent strain, whereas the transformation of plasmid pCN51 had no effect on polyP accumulation in the $\Delta phoU2$ mutant.

TABLE 2 Genes differentially expressed between the Δ *phoU2* mutant and the parent strain

Gene function and gene	GenBank accession no. (location)	Description of product	Fold change in expression by:	
			RNA-Seq	RT-qPCR ^a
Growth				
<i>yycF</i>	NC_002976.3 (2591084–2591786)	DNA-binding response regulator YycF	0.35	0.25 ± 0.08
<i>yycG</i>	NC_002976.3 (2587909–2591072)	Sensor	0.33	0.31 ± 0.14
<i>pflA</i>	NC_002976.3 (2411377–2412133)	Pyruvate formate-lyase-activating enzyme	0.14	0.12 ± 0.02
<i>nrdG</i>	NC_002976.3 (2215127–2217511)	Anaerobic ribonucleoside triphosphate reductase-activating protein	0.31	ND
<i>nrdD</i>	NC_002976.3 (2215127–2217511)	Anaerobic ribonucleoside triphosphate reductase	0.27	0.30 ± 0.14
Biofilm formation				
<i>icaR</i>	NC_002976.3 (2333497–2334055)	Intercellular adhesion regulator	4.58	4.20 ± 1.14
<i>serp0719</i>	NC_002976.3 (713668–716143)	Cell wall surface anchor family protein	0.18	0.13 ± 0.04
<i>rsbU</i>	NC_002976.3 (1724456–1725458)	Sigma factor B regulatory protein	0.31	ND
Autolysis				
<i>serp1880</i>	NC_002976.3 (1904430–1905204)	Secretory antigen precursor SsaA	3.56	ND
<i>serp1884</i>	NC_002976.3 (1909382–1909856)	Secretory antigen precursor SsaA	9.47	ND
<i>serp2120</i>	NC_002976.3 (2144621–2145053)	Secretory antigen precursor SsaA-related protein	1.92	ND
<i>serp2136</i>	NC_002976.3 (2161088–2161862)	Secretory antigen precursor SsaA	3.03	ND
<i>serp0318</i>	NC_002976.3 (322333–323134)	LysM domain-containing protein	1.86	ND
Phosphate transport system				
<i>serp0956</i>	NC_002976.3 (972985–973633)	Phosphate transport system regulatory protein PhoU	5.10	48.95 ± 6.43
<i>serp0957</i>	NC_002976.3 (973639–974515)	Phosphate transporter ATP-binding protein	3.75	67.96 ± 12.14
<i>serp0958</i>	NC_002976.3 (974602–975508)	Phosphate ABC transporter permease	2.29	ND
<i>serp0959</i>	NC_002976.3 (975509–976436)	Phosphate ABC transporter permease	3.32	ND
<i>serp0960</i>	NC_002976.3 (976642–977620)	Phosphate ABC transporter phosphate-binding protein	16.46	ND
<i>serp2283</i>	NC_002976.3 (2323913–2325526)	Phosphonate ABC transporter permease	0.31	ND
<i>serp2284</i>	NC_002976.3 (2323913–2325526)	Phosphonate ABC transporter permease	0.31	ND
<i>serp2285</i>	NC_002976.3 (2325527–2326301)	Phosphonate ABC transporter ATP-binding protein	0.26	ND
<i>serp2286</i>	NC_002976.3 (2326414–2327371)	Phosphonate ABC transporter substrate-binding protein	0.27	ND
<i>serp0317</i>	NC_002976.3 (321130–322141)	Phosphate transporter family protein	0.20	0.35 ± 0.09
<i>malA</i>	NC_002976.3 (1114440–1116096)	Alpha-glucosidase	0.38	ND
<i>lacD</i>	NC_002976.3 (1838482–1839460)	Tagatose-1,6-diphosphate aldolase	0.09	ND
<i>lacA</i>	NC_002976.3 (1840938–1841367)	Galactose-6-phosphate isomerase subunit LacA	0.06	0.13 ± 0.03
<i>lacG</i>	NC_002976.3 (1834966–1836379)	6-Phospho-beta-galactosidase	0.24	0.33 ± 0.07
<i>galU</i>	NC_002976.3 (2080817–2081684)	UTP-glucose-1-phosphate uridylyltransferase	0.47	ND
<i>lacF</i>	NC_002976.3 (1838148–1838463)	PTS system, lactose-specific IIA component	0.12	ND
<i>serp2055</i>	NC_002976.3 (2078963–2080604)	Phosphoglucomutase/phosphomannomutase	0.51	ND
<i>lacC</i>	NC_002976.3 (1839463–1840396)	Tagatose-6-phosphate kinase	0.09	ND
Glycolysis/gluconeogenesis				
<i>gntK</i>	NC_002976.3 (2083340–2084882)	Gluconokinase	0.19	0.33 ± 0.12
<i>pgi</i>	NC_002976.3 (535899–537231)	Glucose-6-phosphate isomerase	0.51	ND
<i>fruK</i>	NC_002976.3 (355255–356931)	1-Phosphofructokinase	21.66	ND
<i>fbaA</i>	NC_002976.3 (1771076–1771937)	Fructose-bisphosphate aldolase	1.74	ND
<i>gapA2</i>	NC_002976.3 (1287162–1288188)	Glyceraldehyde-3-phosphate dehydrogenase	0.62	ND
<i>pgk</i>	NC_002976.3 (447676–448867)	Phosphoglycerate kinase	0.35	ND
<i>gpmA</i>	NC_002976.3 (2023859–2024546)	Phosphoglyceromutase	0.23	ND
<i>ppdK</i>	NC_002976.3 (2199426–2202054)	Pyruvate phosphate dikinase	0.10	0.03 ± 0.01
<i>serp2133</i>	NC_002976.3 (2158590–2159589)	D-Lactate dehydrogenase	1.54	ND
<i>serp2112</i>	NC_002976.3 (2135451–2136504)	Alcohol dehydrogenase	0.03	0.38 ± 0.09
<i>serp2076</i>	NC_002976.3 (2100972–2102937)	Fructose-1,6-bisphosphatase	0.39	ND

(Continued on next page)

TABLE 2 (Continued)

Gene function and gene	GenBank accession no. (location)	Description of product	Fold change in expression by:	
			RNA-Seq	RT-qPCR ^a
Pentose phosphate pathway				
<i>pgi</i>	NC_002976.3 (535899–537231)	Glucose-6-phosphate isomerase	0.51	ND
<i>xylB</i>	NC_002976.3 (2123183–2124674)	D-Xylulose kinase	0.63	ND
<i>gdh</i>	NC_002976.3 (1867994–1868786)	Glucose-1-dehydrogenase	3.52	ND
<i>deoC</i>	NC_002976.3 (1784622–1785397)	Deoxyribose-phosphate aldolase	0.62	ND
<i>prsA</i>	NC_002976.3 (128258–129224)	Ribose-phosphate pyrophosphokinase	0.62	ND
<i>tkt</i>	NC_002976.3 (920891–922880)	Transketolase	0.59	ND
<i>serp2076</i>	NC_002976.3 (2100972–2102937)	Fructose-1,6-bisphosphatase	0.39	ND
<i>gntK</i>	NC_002976.3 (2083340–2084882)	Gluconokinase	0.19	ND
<i>deoB</i>	NC_002976.3 (1781738–1783276)	Phosphopentomutase	0.62	ND
<i>zwf-2</i>	NC_002976.3 (1111611–1113096)	Glucose-6-phosphate 1-dehydrogenase	0.56	ND
<i>serp2055</i>	NC_002976.3 (2078963–2080604)	Phosphoglucomutase/phosphomannomutase	0.51	ND
<i>rpe</i>	NC_002976.3 (788507–789152)	Ribulose-phosphate 3-epimerase	0.65	ND
<i>acnA</i>	NC_002976.3 (932350–935056)	Aconitate hydratase	0.64	ND
<i>icd</i>	NC_002976.3 (1296194–1297463)	Isocitrate dehydrogenase	0.46	ND
<i>serp2324</i>	NC_002976.3 (2360268–2361546)	Branched-chain alpha-keto acid dehydrogenase subunit E2	0.24	ND
<i>sucC</i>	NC_002976.3 (815833–817000)	Succinyl coenzyme A synthetase subunit beta	1.78	ND
<i>sdhB</i>	NC_002976.3 (730805–733414)	Succinate dehydrogenase iron-sulfur subunit	0.20	ND
<i>sdhA</i>	NC_002976.3 (2118832–2119732)	Succinate dehydrogenase flavoprotein subunit	0.17	ND
<i>fumC</i>	NC_002976.3 (1444325–1445711)	Fumarate hydratase	0.51	ND
<i>sucA</i>	NC_002976.3 (1002484–1005289)	2-Oxoglutarate dehydrogenase E1	0.44	ND
<i>sucB</i>	NC_002976.3 (1001203–1002466)	Dihydrolipoamide succinyltransferase	0.25	ND
<i>mqa-3</i>	NC_002976.3 (2350000–2351497)	Malate:quinone oxidoreductase	0.43	ND
<i>mqa-1</i>	NC_002976.3 (1970555–1972034)	Malate:quinone oxidoreductase	0.48	ND
<i>pckA</i>	NC_002976.3 (1409888–1411481)	Phosphoenolpyruvate carboxykinase	0.53	ND
<i>serp0857</i>	NC_002976.3 (868756–869623)	2-Oxoglutarate ferredoxin oxidoreductase subunit beta	0.56	ND
<i>serp0856</i>	NC_002976.3 (866995–868756)	Pyruvate ferredoxin oxidoreductase, alpha subunit	0.44	ND
<i>serp2325</i>	NC_002976.3 (2361559–2362600)	Acetoin dehydrogenase, E1 component, beta subunit	0.33	ND
<i>serp2327</i>	NC_002976.3 (2363665–2365018)	Acetoin dehydrogenase, E3 component, dihydrolipoamide dehydrogenase	1.55	ND
<i>serp1076</i>	NC_002976.3 (1120885–1122205)	2-Oxoisovalerate dehydrogenase E2	0.51	ND
<i>serp1077</i>	NC_002976.3 (1122217–1124192)	2-Oxoisovalerate dehydrogenase E1	0.40	ND
<i>serp1078</i>	NC_002976.3 (1122217–1124192)	2-Oxoisovalerate dehydrogenase E1	0.32	ND
<i>lpdA</i>	NC_002976.3 (1124206–1125628)	2-Oxoisovalerate dehydrogenase E3	0.34	ND
<i>serp2381</i>	NC_002976.3 (2428108–2431126)	NADH:flavin oxidoreductase/fumarate reductase, flavoprotein subunit	0.02	0.082

^aqRT-PCR data are given as the means \pm standard deviations of the results from three independent experiment. ND, not done.

Since polyP in cells can be converted to ATP by phosphotransferases (30) and the transcription of ATP synthase was upregulated in the $\Delta phoU2$ mutant, we determined the intracellular ATP levels in the $\Delta phoU2$ mutant, the $\Delta phoU1$ mutant, and the parent strain using an ATP colorimetric/fluorometric assay kit (Sigma). The intracellular ATP level in the $\Delta phoU2$ mutant was 2.7-fold higher than that in the parent strain ($P < 0.01$) and the $\Delta phoU1$ mutant (Fig. 10B). The amount of ATP recovered from the complemented $\Delta phoU2/pCN51::phoU2$ strain was similar to that recovered from the parent strain.

The expression of genes involved in the pentose phosphate pathway was down-regulated in the $\Delta phoU2$ mutant. Because most of the NADP was generated via PPP and intracellular NADPH, as a reduced form of NADP, plays a very important role in protecting against the toxicity of reactive oxygen species (ROS), intracellular NADPH levels in the $\Delta phoU2$ mutant, the $\Delta phoU1$ mutant, and the parent strain were determined using an NADP/NADPH quantification kit (Sigma). The total amount of NADP in

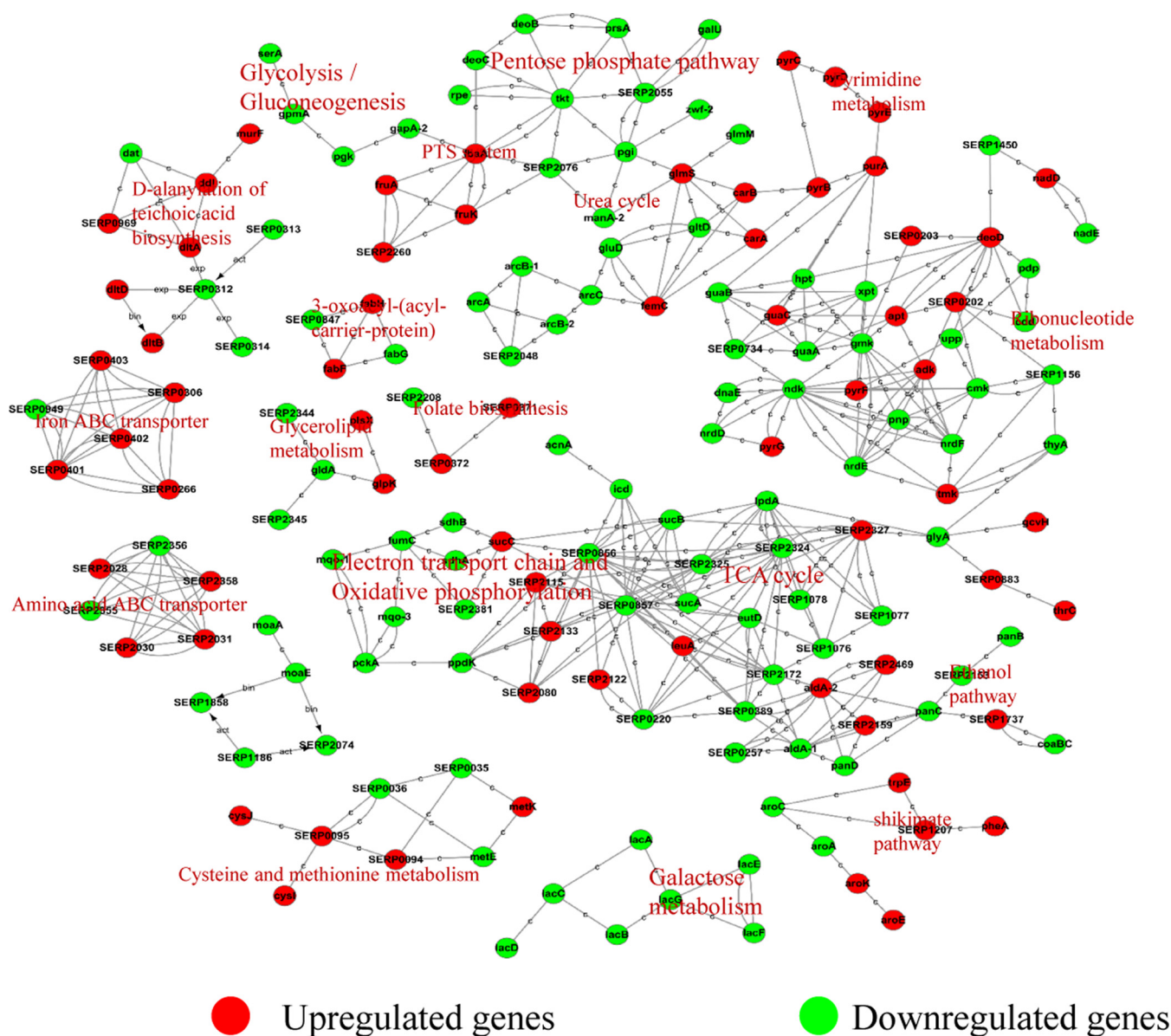


FIG 9 Interaction networks between DEGs identified by transcriptome comparison. The proteins encoded by DEGs (red, green), which were identified by comparison (at 6 h) of the transcriptomes of the $\Delta phoU2$ mutant and the parent strain, were extracted to construct a protein-protein interaction network. The lines in the network represent protein-protein interactions, including binding/association, phosphorylation, activation, and inhibition. Proteins encoded by upregulated and downregulated DEGs are indicated in red and green, respectively.

the $\Delta phoU2$ mutant (A_{450} , 1.041 ± 0.085) was significantly reduced compared with that in the parent strain (A_{450} , 1.691 ± 0.103) ($P < 0.05$) (Fig. 10C), while the amount of NADPH in the $\Delta phoU2$ mutant (A_{450} , 0.014 ± 0.001) was 3-fold lower than that in the parent strain (A_{450} , 0.006 ± 0.001) ($P < 0.01$) (Fig. 10D). The amount of total NADP or NADPH in the $phoU2$ -complemented $\Delta phoU2/pCN51::phoU2$ strain was restored to the level in the parent strain. The reduced content of NADPH in the $\Delta phoU2$ mutant compared with that in the parent strain may have led to the weakened capacity of the $\Delta phoU2$ mutant to withstand oxidative stress. Then, the effects of $phoU2$ on the bacterial response to H_2O_2 were investigated. SDS was also determined to be another stress control. Different concentrations of the bacterial culture were spotted onto TSA containing 6 mM H_2O_2 or 0.006% SDS (8, 31). The $\Delta phoU2$ mutant displayed higher sensitivity to H_2O_2 , and no bacterial survival was detected when 6.4×10^5 CFU was spotted onto plates containing 6 mM H_2O_2 (Fig. 11A); bacteria of the parent strain were

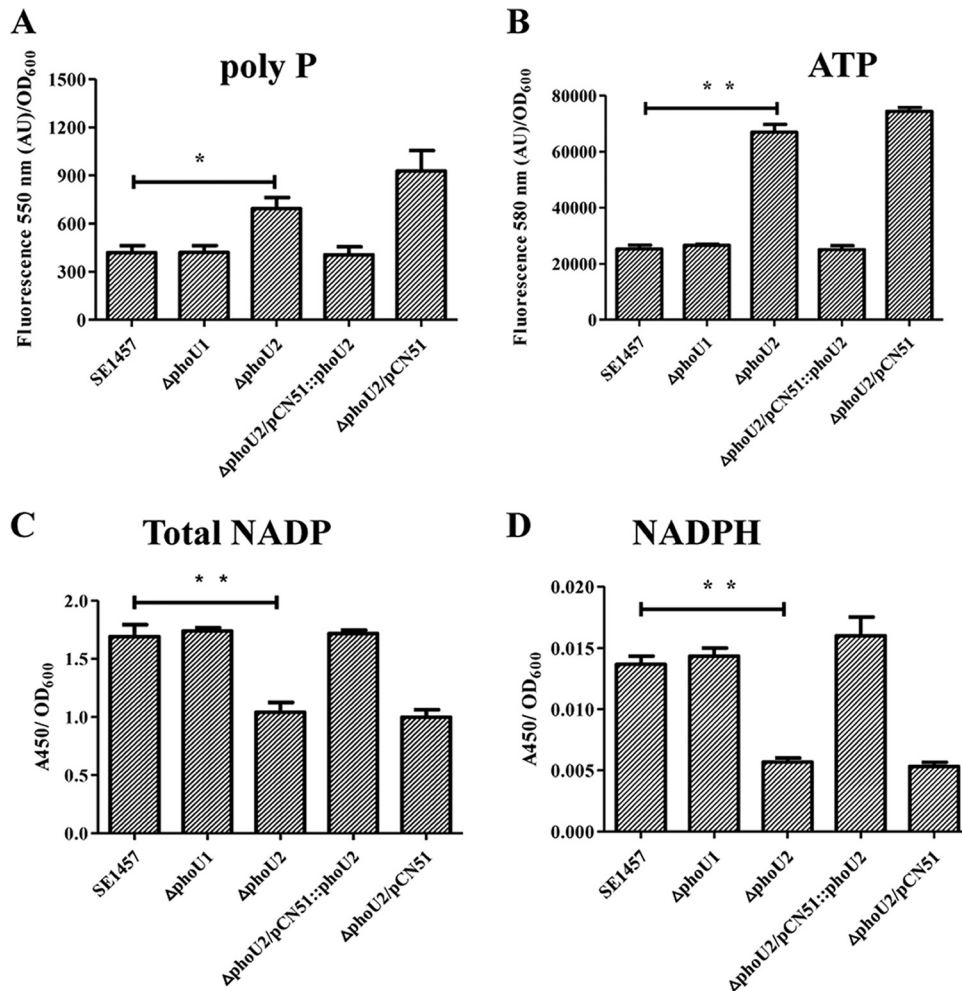


FIG 10 Intracellular polyP, ATP, NADP, and NADPH in the $\Delta phoU2$ mutant. Bacteria were grown to exponential phase in TSB medium. PolyP was assessed by measuring the fluorescence emission of the DAPI-polyP complex at 550 nm. (A) The fluorescence (in arbitrary units [AU]) of the DAPI-polyP complex was measured at 550 nm to evaluate the amount of intracellular polyP. (B) The amount of ATP was determined by measuring the fluorescence emission of the ATP complex at 587 nm. Bacteria were grown to exponential phase in TSB medium ($OD_{600} = 0.5$). (C and D) The amounts of total NADP and NADPH were measured using an NADP/NADPH quantification kit (Sigma). The amounts of total NADP and NADPH were determined by measuring the absorbance of the NADPH complex at 450 nm. Data (means \pm SDs) are from three independent experiments. **, $P < 0.01$; *, $P < 0.05$.

observed at 2.56×10^4 CFU. Complementation of the $\Delta phoU2$ mutant could restore sensitivity to H_2O_2 , the level of which reached that of the parent strain. However, the sensitivity of the $\Delta phoU1$ mutant to H_2O_2 was similar to that of the parent strain. Both the $\Delta phoU1$ mutant and the $\Delta phoU2$ mutant displayed a level of sensitivity to SDS similar to that of the parent strain (Fig. 11B).

DISCUSSION

PhoU in *E. coli* has been identified to be a regulator of phosphate uptake (32–34). Increasing attention has been focused on the regulation of PhoU in bacterial drug tolerance and the stress response. On the basis of the conserved motif of the PhoU protein, two PhoU gene homologs (*serp0956* and *serp0316*) have been identified in *S. epidermidis* and named *phoU1* and *phoU2*, respectively. *phoU1* is located in the *pst* operon and shares a high degree of homology with *phoU* of *E. coli*. *phoU2* (*serp0316*) is cotranscribed with *serp0317* (see Fig. S1 in the supplemental material). *serp0317* is another inorganic phosphate transport gene with homology to *pit* in *E. coli* (35, 36). Using bioinformatics analysis, the genome of *S. aureus* (NCTC8325) was found to

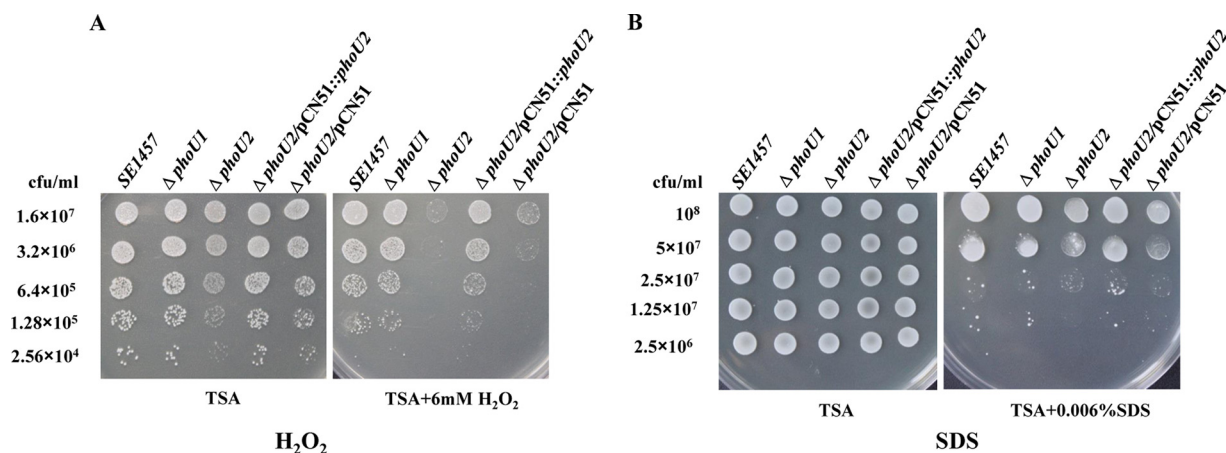


FIG 11 Sensitivity of the $\Delta phoU1$ and $\Delta phoU2$ mutants to H_2O_2 and SDS. Overnight cultures of the bacterial strains were diluted 1:200 in fresh TSB medium and incubated at 37°C with aeration for 3 h until the OD_{600} was approximately 2. After 2-fold serial dilution, each 5- μ l aliquot was spotted onto a TSA agar plate containing 6 mM H_2O_2 or 0.006% SDS and incubated overnight at 37°C. The growth of colonies on plates containing H_2O_2 or SDS was photographed.

contain two PhoU gene homologs (*SAOUHSC_01384* and *SAOUHSC_00669*). *phoU2* of *S. epidermidis* shares 86% identity with *SAOUHSC_00669* at the nucleotide sequence level and PhoU2 shares 97% identity at the amino acid sequence level with *SAOUHSC_00669* in *S. aureus*. *SAOUHSC_00669* has been investigated as a gene required for the sensitivity of an *S. aureus* strain with a point mutation in *pitA* (*SAOUHSC_00670*) to daptomycin (11, 12).

The number of PhoU homologs varies in different bacterial species. In *E. coli*, *P. aeruginosa*, and *Streptococcus pneumoniae*, there is only one PhoU, while in *T. maritima*, *M. tuberculosis*, *M. marinum*, *S. aureus*, and *S. epidermidis*, two PhoU homologs have been identified. In *E. coli*, *phoU* plays an important role in polyP accumulation (34) and the formation of multidrug-resistant bacteria (5, 34). In *P. aeruginosa*, PhoU is a negative regulator of intracellular ppGpp and polyP. However, *phoU* mutation has no effect on *P. aeruginosa* biofilm formation (8). In species of mycobacteria, there are two *phoU* homologs, *phoY1* and *phoY2*. *phoY2* has been investigated as the functional homolog of *phoU*, regulating the generation of multidrug-tolerant bacteria and maintaining metabolic homeostasis and adaptation to stress conditions in *M. tuberculosis* and *M. marinum* (6, 7).

Alignment of the amino acid sequences of PhoU1 and PhoU2 from *S. epidermidis* RP62A, PhoU from *E. coli* K-12, and the two PhoU homologs (PhoY1 and PhoY2) from *M. tuberculosis* H37Rv showed that the metal ion-binding sites are conserved in all the PhoU homologs (Fig. S2). To investigate the regulatory functions of the *phoU* homologs, the $\Delta phoU1$ and $\Delta phoU2$ mutants of the *S. epidermidis* 1457 strain were constructed and the transcriptomes of the deletion mutants and the parent strain were compared. We detected the transcription levels of *phoU1* (*SERP0956*) and *phoU2* (*SERP0316*) in SE1457 by RT-qPCR at different time point (4 h, 6 h, 8 h, 10 h, and 12 h), and both *phoU1* and *phoU2* of SE1457 were expressed at the time points evaluated (Fig. S1). In logarithmic phase (6 h), 945 genes were differentially expressed between the $\Delta phoU2$ mutant and the parent strain; among these, 474 were upregulated and 471 were downregulated. However, only 92 DEGs were detected between $\Delta phoU1$ and the parent strain during logarithmic phase and 2 DEGs were detected during stationary phase. On the basis of Gene Ontology analysis of the genes differentially expressed between the $\Delta phoU1$ mutant and the parent strain, 23 DEGs that were downregulated in the $\Delta phoU1$ mutant were involved in translation, ribosomal structure, and biogenesis, while 69 upregulated DEGs were involved in 17 pathways or metabolic processes. However, the differences in the levels of expression of none of these DEGs were statistically significant ($P > 0.05$). It is worth mentioning that the *pst* operon was not identified among the genes

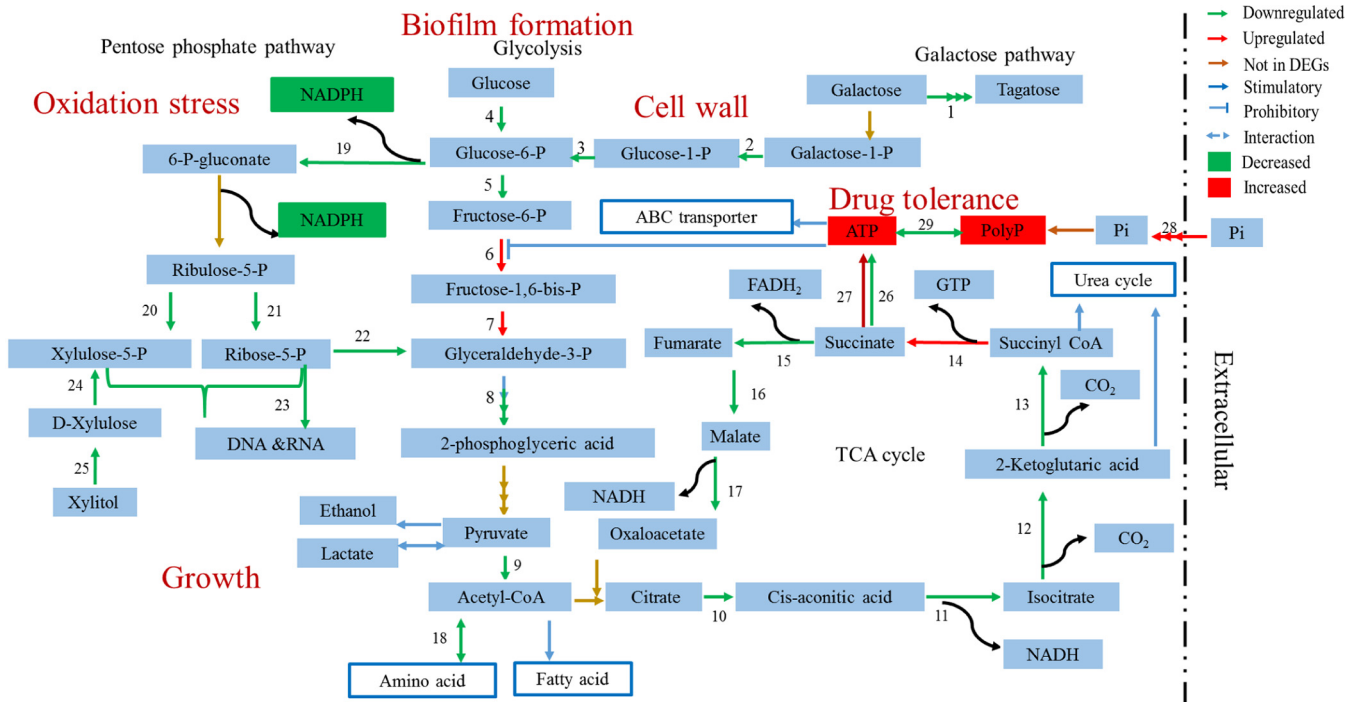


FIG 12 Major metabolic pathways in the $\Delta phoU2$ mutant revealed by DEGs. Shown are transcription of enzyme-encoding genes that were downregulated and upregulated, enzyme-encoding genes that were not found in DEGs (genes differentially expressed between the $\Delta phoU2$ mutant and the parent strain), stimulatory reactions, prohibitory reactions, reversible reaction interactions between the two products, and products whose amounts were increased or decreased. The numbers represent the enzyme-encoding genes listed in Table 3. P, phosphate; CoA, coenzyme A.

differentially expressed between the $\Delta phoU1$ mutant and the parent strain, and the results were validated by RT-qPCR. Hence, in this study, we focused on investigating *phoU2* functions in *S. epidermidis*.

The $\Delta phoU2$ mutant of *S. epidermidis* displayed growth retardation under both microaerobic and oxic conditions, in accordance with the findings in an *E. coli* strain with a PhoU deletion (37). The deletion of *phoU1* had no effect on bacterial growth. Analysis of the DEGs (genes differentially expressed between the $\Delta phoU2$ mutant and the parent strain) showed that in the $\Delta phoU2$ mutant, the expression of *pflA* and *nrdDG* was downregulated. These genes are involved in the growth of *S. epidermidis* under microaerobic conditions. PflA is an enzyme activating PflB, a pyruvate formate-lyase that catalyzes the reversible conversion of pyruvate to formate, thereby producing acetyl coenzyme A. Thus, PflA plays an important role in utilization of the energy supply when pyruvate is available and favors the growth of cells under fermentation conditions (18). The protein encoded by *nrdDG* is a class III ribonucleotide reductase that catalyzes the synthesis of deoxynucleoside triphosphates (dNTPs) via the reduction of nucleoside triphosphates under anaerobic conditions (38–40). In the $\Delta phoU2$ mutant, the expression of *ycyFG* is significantly downregulated ($P < 0.01$); *ycyFG* is an essential two-component system in Gram-positive bacteria that regulates cell wall metabolism, cell division, virulence, and biofilm formation (41, 42). Expression of the essential two-component system *ycyFG* was downregulated during the logarithmic phase but was not detected during the stationary phase. This finding is in accordance with the results of the assessments of the $\Delta phoU2$ mutant under the different growth conditions. In addition, the downregulated expression of DEGs involved in the TCA cycle, glycolysis and gluconeogenesis, and the pentose phosphate pathway may promote growth retardation (Fig. 12 and Table 3). The growth retardation of the $\Delta phoU2$ mutant did not persist to stationary phase, as there were no differences in the CFU counts from those of the parent strain in stationary phase.

S. epidermidis is an important nosocomial pathogen that forms biofilms on im-

TABLE 3 DEGs involved in major metabolic pathway

DEG no.	Gene name(s)	Enzyme(s) encoded
1	<i>lacA, lacD, lacG</i>	Galactose-6-phosphate isomerase subunit LacA, tagatose-1,6-diphosphate aldolase, 6-phospho-beta-galactosidase
2	<i>galU</i>	UTP-glucose-1-phosphate uridylyltransferase
3	<i>serp2055</i>	Phosphoglucomutase/phosphomannomutase
4	<i>gntK</i>	Gluconokinase
5	<i>pgi</i>	Glucose-6-phosphate isomerase
6	<i>fruK</i>	1-Phosphofructokinase
7	<i>fbaA</i>	Fructose-bisphosphate aldolase
8	<i>gapA2, pgk, gpmA</i>	Glyceraldehyde-3-phosphate dehydrogenase, phosphoglycerate kinase, phosphoglyceromutase
9	<i>serp0856, serp0857</i>	2-Oxoglutarate ferredoxin oxidoreductase subunit beta, pyruvate ferredoxin oxidoreductase, alpha subunit
10	<i>acnA</i>	Aconitate hydratase
11	<i>acnA</i>	Aconitate hydratase
12	<i>icd</i>	Isocitrate dehydrogenase
13	<i>serp2324</i>	Branched-chain alpha-keto acid dehydrogenase subunit E2
14	<i>sucC</i>	Succinyl coenzyme A synthetase subunit beta
15	<i>sdhA, sdhB</i>	Succinate dehydrogenase iron-sulfur subunit, succinate dehydrogenase flavoprotein subunit
16	<i>fumC</i>	Fumarate hydratase
17	<i>mgo-1, mgo-3</i>	Malate:quinone oxidoreductase, malate:quinone oxidoreductase
18	<i>serp1076, serp1077, serp1078, lpdA</i>	2-Oxoisovalerate dehydrogenase E2, 2-oxoisovalerate dehydrogenase E1, 2-oxoisovalerate dehydrogenase E1, 2-oxoisovalerate dehydrogenase E3
19	<i>zwf-2</i>	Glucose-6-phosphate 1-dehydrogenase
20	<i>rpe</i>	Ribulose-phosphate 3-epimerase
21	<i>deoB</i>	Phosphopentomutase
22	<i>deoC</i>	Deoxyribose-phosphate aldolase
23	<i>prsA</i>	Ribose-phosphate pyrophosphokinase
24	<i>xylB</i>	D-Xylulose kinase
25	<i>tkt</i>	Transketolase

planted medical devices. We studied the regulatory role of *phoU2* in this respect. The Δ *phoU2* mutant exhibited impaired biofilm formation under both static and hydrodynamic conditions, in contrast to the findings obtained for *P. aeruginosa*. A study performed in 2015 found that inactivation of *phoU* had no effect on the formation of bacterial biofilms in *P. aeruginosa* (8). In the Δ *phoU2* mutant, the expression of the sigma factor B regulator gene (*rsbU*), involved in biofilm formation, is downregulated ($P < 0.01$) (20). In addition, the downregulation of genes that participate in galactose metabolism plays an essential role in *Bacillus subtilis* biofilm formation. The intermediate product of galactose metabolism, UDP-galactose, is used in the synthesis of exopolysaccharide (EPS) of the biofilm matrix in *B. subtilis* (43). In accordance with these phenomena, the production of Aap was decreased in the Δ *phoU2* mutant. Defective attachment of the Δ *phoU2* mutant could be another important reason for the reduced biofilm formation. The decreased biofilm formation was not due to growth retardation, as the number of CFU of the Δ *phoU2* mutant during the stationary phase was similar to that of the parent strain, and the time required for biofilm formation was extended to 48 h.

The downregulated expression of genes involved in the TCA cycle, glycolysis, and gluconeogenesis resulted in a lack of polysaccharide, which was also responsible for the biofilm formation defect in the Δ *phoU2* mutant.

The Δ *phoU2* mutant of *S. epidermidis* displayed a rough cell wall and rapid autolysis. The rough cell wall may indicate that the cell wall of the Δ *phoU2* mutant was incomplete, potentially due to the low expression levels of the galactose metabolism genes. The intermediate products of galactose metabolism are involved in the synthesis of peptidoglycan. Peptidoglycan, which is also known as murein, is the most important component of Gram-positive bacterial cell walls (Fig. 12). In addition to the autolysis genes, *ssaA* and *serp0318* were upregulated in the Δ *phoU2* mutant; the incomplete cell wall may have led to the rapid autolysis in the Δ *phoU2* mutant (22, 23). Besides the peptidoglycan, the level of another component of the cell wall, teichoic acid, may also have been decreased in the Δ *phoU2* mutant. Teichoic acids are special components in

the cell wall of most Gram-positive bacteria, such as species in the genera *Staphylococcus*, *Streptococcus*, and *Bacillus*. Teichoic acids are bacterial copolymers of glycerol phosphate or ribitol phosphate and carbohydrates linked via phosphodiester bonds and are the essential product of glycolysis or the pentose phosphate pathway. The downregulation of glycolysis or the pentose phosphate pathway in the $\Delta phoU2$ mutant may reduce the level of production of teichoic acids, which would result in a rough cell surface and an increase in autolysis capacity (44, 45).

Inorganic phosphate (P_i) is an important macronutrient for all living organisms, comprising up to 3% of the bacterial dry weight, and is involved in many important pathways (8). The expression of genes in the *pst* operon and *serp0317* was upregulated in the $\Delta phoU2$ mutant, which is consistent with the intracellular accumulation of polyP in the $\Delta phoU2$ mutant. A portion of the inorganic phosphate taken up from the environment was used for bacterial metabolism, and redundant inorganic phosphate was stored as high-molecular-weight inorganic polyphosphate (polyP) in bacterial cells (46) (Fig. 12). PolyP is a linear polymer composed of several molecules of orthophosphate (P_i) that are linked by energy-rich phosphoanhydride bonds (30). PolyP is a known stress response molecule that accumulates in microorganisms in response to nutrient deprivation, high salt concentrations, or other environmental stress conditions (30, 47). An imbalance in the amount of intracellular polyP in *E. coli* elicits a defective response to oxidative, osmotic, and thermal stresses (5, 34). In *M. tuberculosis*, a *phoY2* transposon insertion mutant accumulates large amounts of polyP and has an increased sensitivity to thermal stress, H_2O_2 , and antibiotics (6, 7). The characteristics of phosphate metabolism in the *S. epidermidis* $\Delta phoU2$ mutant are similar to those in *phoU* deletion mutants or insertion inactivation mutants of *E. coli*, *P. aeruginosa*, *M. tuberculosis*, and *M. marinum* (5–8).

To study the regulation of phosphate metabolism by PhoU1 and PhoU2, we determined the intracellular inorganic phosphate content and the growth of the PhoU mutants (the $\Delta phoU1$ and $\Delta phoU2$ mutants), in addition to the amount of polyP, under phosphate-limiting conditions. There were no differences in the intracellular inorganic phosphate content between the PhoU mutants and the parent strain (SE1457) (Fig. S3B). The growth curves of the PhoU mutants under P_i -limiting conditions were similar to those of the mutants cultured in TSB medium (P_i -replete conditions) (Fig. S3A). Comparison of the transcriptomes of the PhoU mutants and the parent strain showed that the transcription of the *pst* operon was upregulated in the $\Delta phoU2$ mutant, which suggests that phosphate uptake was increased in the $\Delta phoU2$ mutant and the extra phosphate was utilized to synthesize polyP to maintain the intracellular inorganic phosphate at a level similar to that in SE1457. However, in the $\Delta phoU1$ mutant there was no difference in the level of *pst* operon expression, the intracellular inorganic phosphate and polyP content, or growth under P_i -limiting conditions compared with the findings for SE1457. These results suggest that PhoU2 but not PhoU1 plays an important role in the homeostasis of intracellular P_i .

The polyP in bacterial cells could be converted to ATP by phosphotransferases. In addition, among the genes differentially expressed between the $\Delta phoU2$ mutant and the parent strain, the expression of genes encoding ATP synthase was upregulated. Thus, we verified that the levels of intracellular ATP were higher in the $\Delta phoU2$ mutant strain than the parent strain, which is consistent with the results obtained for *M. marinum* (7). ATP is the most important energy-providing substrate. A high level of intracellular ATP influences the expression of many genes and metabolic pathways, such as the genes for ATP-binding cassette (ABC) transporters. ABC transporters utilize the energy from ATP binding and hydrolysis to transport various substrates, including ions, amino acids, peptides, sugars, and other molecules, across cellular membranes (48). Excessive ABC transporter activity would result in an imbalance in the uptake of substances. A high level of ATP would maintain cellular metabolism at an unhealthy active level (49). Under this condition, bacteria are easily killed by bactericidal antibiotics. Therefore, *S. epidermidis* $\Delta phoU2$ showed a reduced drug tolerance compared with the wild-type strain (Fig. 12).

On the basis of the protein-protein interaction network developed for the proteins encoded by the DEGs, 174 proteins encoded by DEGs were found to be involved in various metabolic pathways, such as the pentose phosphate pathway, the TCA cycle, and galactose metabolism. Among these, the expression of all genes that participate in the pentose phosphate pathway was downregulated in the $\Delta phoU2$ mutant. We found that the amount of NADPH in the $\Delta phoU2$ mutant decreased 3-fold compared with that in the parent strain. NADPH is produced mainly via the pentose phosphate pathway, which parallels the glycolysis pathway. The pentose phosphate pathway generates NADPH and pentoses (5-carbon sugars) as well as ribose-5-phosphate. NADPH provides the reducing equivalents for biosynthetic reactions and the oxidation-reduction involved in protection against the toxicity of reactive oxygen species (ROS), allowing the regeneration of glutathione (GSH) (24–29). The decreased NADPH in the $\Delta phoU2$ mutant corresponded to its high sensitivity to H_2O_2 (Fig. 12). The major product of PPP is ribose-5-phosphate, a precursor for the synthesis of nucleotides (DNA and RNA). The reduced synthesis of ribose-5-phosphate led to a lack of DNA and RNA, and this reduced amount of ribose-5-phosphate might be responsible for the growth retardation seen in the $\Delta phoU2$ mutant (Fig. 12).

To confirm the role of *phoU2* on the regulation of growth and biofilm formation in SE1457, we used the antisense technology to test the effect of silencing of *phoU2* expression on the $\Delta phoU1$ mutant. First, we constructed a plasmid which could express *phoU2* antisense RNA (AS-*phoU2*) in the presence of 250 ng/ml anhydrotetracycline (ATc), and the plasmid was transferred to the $\Delta phoU1$ mutant to obtain the AS-*phoU2* $\Delta phoU1$ mutant. After induction with ATc, the transcription level of *phoU2* was reduced to 10% in the AS-*phoU2* $\Delta phoU1$ mutant compared with that in the $\Delta phoU1$ mutant. The AS-*phoU2* $\Delta phoU1$ mutant displayed a level of growth retardation that was the same as that in the $\Delta phoU2$ mutant (Fig. S4A), while the level of biofilm formation was less than that in the $\Delta phoU1$ mutant carrying the vector pMX6 ($P < 0.01$) (Fig. S4B).

In summary, *phoU2* regulates growth, biofilm formation, oxidative stress, and drug tolerance via some important pathways and processes, including the pentose phosphate pathway, glycolysis, the TCA cycle, inorganic phosphate metabolism, galactose metabolism, and ABC transporter activity in SE1457. However, no obvious phenotype of the $\Delta phoU1$ mutant was observed in the presence of *phoU2* in SE1457. The mechanism of *phoU2* regulation and the interaction between *phoU1* and *phoU2* in SE1457 warrant further investigation.

The effects of PhoU1 and PhoU2 on biofilm formation and antibiotic tolerance in *S. epidermidis* clinical strains need to be further studied by the use of gene knockout or antisense RNA technology.

MATERIALS AND METHODS

Bacterial strains, plasmids, growth conditions, and chemicals. All of the bacterial strains and plasmids used in the study are shown in Table 4. The biofilm-positive strain *S. epidermidis* ATCC 35984 (RP62A; GenBank accession number [NC_002976](#)) and non-biofilm-forming strain ATCC 12228 (GenBank accession number [NC_004461](#)) were purchased from the American Type Culture Collection (ATCC; Manassas, VA) (50). *S. epidermidis* 1457 (SE1457) and *S. aureus* RN4220 were provided by Gao Fu from the University of Hong Kong. The *S. epidermidis* strains and *S. aureus* RN4220 were cultured in tryptic soya broth (TSB; Oxoid, Basingstoke, UK) at 37°C with shaking at 220 rpm. Glucose was added to the TSB medium at a concentration of 0.5% for the detection of biofilm formation. Electroporation was used for plasmid transformation, and B2 medium (1% casein hydrolysate, 2.5% yeast extract, 0.5% glucose, 2.5% NaCl, 0.1% K_2HPO_4 , pH 7.5) was used for the recovery of bacteria. The antibiotics used in this study were purchased from Sigma Chemical Co. (Los Angeles, CA, USA) and used at concentrations of 10 mg/liter for chloramphenicol, 100 mg/liter for ampicillin, 50 ng/ml for anhydrotetracycline, and 10 mg/liter for erythromycin.

Construction of $\Delta phoU1$ and $\Delta phoU2$ mutants and complemented strains. The *phoU1* and *phoU2* deletion mutants of the SE1457 strain were constructed by allelic replacement using the temperature-sensitive plasmid pKOR1 as described by Bae and Schneewind (51). Briefly, the upstream and downstream fragments of *phoU1* and *phoU2* were amplified by PCR and separately cloned into the pKOR1 vector, resulting in pKOR1- $\Delta phoU1$ and pKOR1- $\Delta phoU2$. The recombinant plasmid pKOR1- $\Delta phoU$ was successively transferred into *E. coli* DH5 α , *S. aureus* RN4220, and then SE1457, followed by allelic replacement as described previously (52, 53). The *phoU1* and *phoU2*

TABLE 4 Bacterial strains and plasmids used in the present study

Bacterial strain or plasmid	Description	Source
Bacterial strains		
<i>S. epidermidis</i> 1457	Clinical strain, biofilm positive	
Δ <i>phoU1</i> mutant	<i>phoU1</i> deletion mutant obtained using SE1457 as the parent strain	This study
Δ <i>phoU2</i> mutant	<i>phoU2</i> deletion mutant obtained using SE1457 as the parent strain	This study
Δ <i>phoU2/pCN51::phoU2</i>	<i>phoU2</i> mutant complemented with plasmid pCN51 harboring the <i>phoU2</i> gene	This study
Δ <i>phoU2/pCN51</i>	<i>phoU2</i> mutant complemented with plasmid pCN51	This study
<i>S. epidermidis</i> RP62A	Standard strain, biofilm positive	ATCC
<i>S. epidermidis</i> ATCC 12228	Standard strain, biofilm negative	ATCC
<i>S. aureus</i> RN4220	Restriction-deficient strain permitting shuttle of a plasmid modified by its host specificity determination from Gram-negative to Gram-positive bacteria	Gao Fu, University of Hong Kong
Plasmids		
pKOR1	Temp-sensitive <i>E. coli</i> (Amp ^r)- <i>Staphylococcus</i> (Cm ^r) shuttle vector	Li Min, Institute of Antibiotics, Huashan Hospital
pKOR1- Δ <i>phoU1</i>	Recombinant plasmid	This study
pKOR1- Δ <i>phoU2</i>	Recombinant plasmid	This study
pCN51	A Cd ²⁺ -inducible shuttle plasmid, Erm ^r	Wageningen University, Holland
pCN51- <i>phoU2</i>	A Cd ²⁺ -inducible shuttle plasmid, Erm ^r ; the <i>phoU2</i> gene was cloned into plasmid pCN51	This study

deletion mutants were verified by PCR, RT-qPCR, and direct sequencing and are referred to as the Δ *phoU1* and Δ *phoU2* mutants. The complemented Δ *phoU2* mutant strain was constructed using a shuttle vector, pCN51 (54). The *phoU2* gene and its Shine-Dalgarno region were amplified by PCR using primers *phoU2*-BamHI-F/*phoU2*-KpnI-R, whose sequences are provided in Table 5. Plasmid pCN51-*phoU2* was used for complementation and was constructed by inserting a fragment of the digested PCR products of the *phoU2* gene with BamHI and KpnI (55). Plasmid pCN51-*phoU2* was transformed by electroporation into the Δ *phoU2* mutant, forming the complemented Δ *phoU2/pCN51::phoU2* strain. The Δ *phoU2* strain containing the empty vector pCN51 was designated the Δ *phoU2/pCN51* mutant. The primers used in this assay are listed in Table 5.

Growth curves of the Δ *phoU1* and the Δ *phoU2* mutant strains. The SE1457, Δ *phoU1*, Δ *phoU2*, Δ *phoU2/pCN51::phoU2*, and Δ *phoU2/pCN51* strains were cultured in TSB at 37°C with shaking for 12 h.

TABLE 5 Primers used in this study

Primer use and primer ^a	Primer sequence (5'–3')	Location ^b	Size of PCR product (bp)	Note ^c
Construction of Δ <i>phoU1</i> mutant				
<i>phoU1</i> us-F	GGGGACAAGTTTGTACAAAAAGCAGGCTAAATGCCTCAAGCAGAATTC	974705–974724	1,061	<i>attB1</i>
<i>phoU1</i> us-R	GGGGTACCAATTGCCATTGCATCTTATCC	973625–973645		KpnI
<i>phoU1</i> ds-F	GGGGTACCGATTAATTAATCAATCC TATTG	972969–972991	823	KpnI
<i>phoU1</i> ds-R	GGGGACCACTTTGTACAAGAAAGCTGGGTTTGCTCAGAATAAAGGAAAAG	972127–972147		<i>attB2</i>
Construction of Δ <i>phoU2</i> mutant				
<i>phoU2</i> us-F	GGGGACAAGTTTGTACAAAAAGCAGGCTGTTGATCGTGGTAGACCG	319402–319419	1,100	<i>attB1</i>
<i>phoU2</i> us-R	GGGGTACCCATTAATAATCC TCCATTTTGA	320480–320501		KpnI
<i>phoU2</i> ds-F	GGGGTACCTAAGGGAGCTTTATTTATGTC	321114–321135	959	KpnI
<i>phoU2</i> ds-R	GGGGACCACTTTGTACAAGAAAGCTGGGTACCCATGTTACAACCATAC	322053–322072		<i>attB2</i>
Construction of Δ <i>phoU2</i> complemented strain				
<i>phoU2</i> -BamHI-F	CGCGGATCCGTAATCAGTTCCTCA			BamHI
<i>phoU2</i> -KpnI-R	CGGGGTACCTAAATAAAGACTCCCT			KpnI
RT-qPCR				
<i>gyrB</i> F	AGAAGAGGAAGTTAGAGAAGA	2611073–2611093	168	
<i>gyrB</i> R	GCATATCC ACTGTTATATTGAAG	2610926–2610948		
<i>phoU1</i> F	CGTCTTGGTCTTCGTGTA	973556–973573	169	
<i>phoU1</i> R	CAATAGGTTGTTGTCTCGTAAT	973405–973426		
<i>phoU2</i> F	GCTGTAGGATTACTTGTAGAC	320874–320894	200	
<i>phoU2</i> R	GCTTGACACTTATCTGCTATT	321073–321053		

^aPrimers were designed according to the genomic sequence of *S. epidermidis* RP62A (GenBank accession number [NC_002976](https://www.ncbi.nlm.nih.gov/nuccore/NC_002976)). F, forward primer; R, reverse primer.

^bLocation of the primer in the genomic sequence of *S. epidermidis* RP62A.

^cThe underlined sequences represent the BP reaction sites or restriction enzyme sites.

Overnight cultures of the *S. epidermidis* strains were diluted (1:200) in 10 ml TSB in a 100-ml flask and incubated at 37°C under aerobic or microanaerobic conditions with shaking at 220 rpm. The OD₆₀₀ was measured using a UV spectrophotometer (Eppendorf, Hamburg, Germany) (53).

Morphology of the $\Delta phoU1$ and $\Delta phoU2$ mutants observed by TEM. The SE1457, $\Delta phoU1$, $\Delta phoU2$, $\Delta phoU2/pCN51::phoU2$, and $\Delta phoU2/pCN51$ strains were cultured in TSB at 37°C for 6 h. The log-phase bacteria were rinsed with phosphate-buffered saline (PBS), prefixed with 2.5% glutaraldehyde at 4°C for 2 h, and then fixed in 1% osmium for 3 h. The fixed samples were dehydrated in a graded ethanol series, embedded in epoxy resin, and stained with uranyl acetate and lead citrate. Ultrathin sections were cut with a Leica Ultracut microtome and observed under a transmission electron microscope (TEM; Philips Tecnai-12 Biotwin). TEM micrographs were separately obtained at magnifications of $\times 11,500$ and $\times 26,500$ (56, 57).

Microtiter plate assay of biofilm formation. The biofilm-forming ability of the strains was assessed using a semiquantitative microtiter plate assay, based on the protocol described by Christensen et al. (58). Briefly, overnight cultures of the *S. epidermidis* strains were diluted (1:200) into fresh TSB (containing 0.5% glucose). Aliquots of the diluted cultures were inoculated into polystyrene 96-well flat-bottomed microtiter plates (Costar; Corning, USA) and incubated at 37°C for 6 h, 12 h, 24 h, or 48 h. After the planktonic cultures were decanted, the plates were gently rinsed three times with PBS. The biofilms were fixed with 99% methyl alcohol for 15 min, stained with 2% crystal violet for 5 min, rinsed with running tap water, and air dried at room temperature. The optical densities at 570 nm (OD_{570s}) of the plates were then determined using a spectrophotometer (DTX880; Beckman Coulter, Fullerton, CA) (52). The biofilm formation by each strain was assessed three times using strains ATCC 12228 and ATCC 35984 as non-biofilm-forming and biofilm-forming controls, respectively.

CLSM of biofilms. An overnight culture of each *S. epidermidis* strain (1:200 dilution) was inoculated into 2 ml TSB (with 0.5% glucose supplementation) in a cell culture dish containing a glass coverslip (World Precision Instruments, USA) (59, 60). After culturing under static conditions at 37°C for 24 h, the dish was gently washed three times with saline and then stained with LIVE/DEAD reagents (1 μ M SYTO9 and 1 μ M propidium iodide [PI]; Thermo Fisher Scientific, Houston, TX) for 20 min and observed using a confocal laser scanning microscope (CLSM; TCS-SP5, Leica, Germany) with a 63 \times oil immersion objective (numerical aperture, 1.4). Photomicrographs of the biofilms were generated using Leica LAS AF software. Three-dimensional images were created using IMARIS (version 7.0.0) software (Bitplane). The live and dead bacteria were quantified using ImageJ software. Three independent experiments were performed.

Flow-based biofilm assays. A BioFlux 1000 system (Fluxion Biosciences) with a Leica microscope and temperature-controlled housing was used for all imaging experiments. Automated microscopy and image processing were performed using BioFlux Montage software. BioFlux 48-well plates (catalog no. 910-0047; Fluxion Biosciences) allowing up to 24 individual treatment conditions were primed with TSB from the inlet well at a shear setting of 2 dynes/cm² for 10 min. Cultures of *S. epidermidis* were grown to mid-log phase and normalized to an OD₆₀₀ of 0.15. Bacteria were seeded from the outlet well into the channel and viewing window at a shear setting of 2 dynes/cm² for 3 s. After 1 h of incubation at 37°C, TSB was set to flow from the inlet well at a shear setting of 0.15 dyne/cm² for the duration of the experiment. Images were automatically acquired every 10 min at multiple stage positions using bright-field illumination; images were also acquired in the red channel (tetramethyl rhodamine isothiocyanate [TRITC] filter set; catalog no. 86013v2; Chroma, Bellows Falls, VT) using a 200-ms exposure time. The background-corrected average pixel intensity per image was used to quantify biofilm formation (61).

Autolysis of the $\Delta phoU1$ and $\Delta phoU2$ mutants induced by Triton X-100. Autolysis assays were performed as described by Brunskill and Bayles with minor modifications (62). Briefly, the *S. epidermidis* strains were cultured in TSB (containing 1 M NaCl) to mid-exponential phase (6 h) and harvested by centrifugation (4,000 $\times g$, 4°C, 15 min). After the bacterial pellets were washed with ice-cold water, they were resuspended to an OD₆₀₀ of 1.0 in lysis buffer (50 mM Tris-HCl buffer, pH 8.0, containing 0.05% Triton X-100) and incubated at 30°C with shaking at 200 rpm. The optical density at 600 nm was measured at 30-min intervals for 3 h (59).

Initial adherence capacity of the $\Delta phoU1$ and $\Delta phoU2$ mutants. Primary attachment of the $\Delta phoU1$ and $\Delta phoU2$ strains to a polystyrene surface was assessed as described previously, with modifications (52, 53, 59). Briefly, overnight cultures of the SE1457, $\Delta phoU1$, $\Delta phoU2$, $\Delta phoU2/pCN51::phoU2$, and $\Delta phoU2/pCN51$ strains were inoculated into TSB and cultured at 37°C to logarithmic phase (OD₆₀₀ \approx 0.6). The bacterial culture was adjusted to an OD₆₀₀ of 0.1 with PBS and inoculated into six-well plates (2 ml/well; Nunc, Roskilde, Denmark). After incubation at 37°C for 2 h, the plates were washed gently with PBS and observed under a microscope using a 40-fold objective lens. The numbers of attached cells in each photomicrograph were counted using ImageJ software, and three microscopic fields were observed per sample.

Assay of PIA in biofilms. Polysaccharide intercellular adhesion (PIA) in the biofilms of the $\Delta phoU1$ and $\Delta phoU2$ mutants was semiquantified by a dot blot assay with a wheat germ agglutinin (WGA)-horseradish peroxidase (HRP) conjugate as described previously (63, 64). Briefly, overnight cultures of the *S. epidermidis* strains were inoculated into six-well plates (Nunc) and incubated at 37°C for 24 h. Biofilms were scraped off the bottoms of the wells, resuspended in 0.5 M EDTA, and centrifuged (13,000 $\times g$, 5 min) after they were heated at 100°C for 5 min. The supernatant was treated with proteinase K (20 mg/ml) at 37°C for 3 h and inactivated at 100°C for 5 min. Serial dilutions of the PIA assay extract were transferred to a nitrocellulose membrane (Millipore, Billerica, MA) using a 96-well dot blot device

(Biometra GmbH, Göttingen, Germany). The air-dried membrane was blocked with 5% (wt/vol) skim milk and subsequently incubated with the WGA (3.2 $\mu\text{g/ml}$)-HRP conjugate for 1 h (Lectinotest Laboratory, Lviv, Ukraine). HRP activity was visualized by chromogenic detection using 4-chloride-1-naphthol (Sigma) as the substrate. Quantitation of PIA was represented as the highest dilution of the supernatant in which HRP was detectable.

Detection of Aap. Accumulation-associated protein (Aap) expression by the ΔphoU1 and ΔphoU2 strains was determined by Western blotting with an Aap-specific monoclonal antibody (MAB₁₈₈₆) that was generated in our laboratory (60). Briefly, 24-h-old biofilms of the *S. epidermidis* strains were collected and adjusted to an identical OD₆₀₀ after they were washed with PBS. The bacteria were treated with lysostaphin (Sigma) and centrifuged (20,000 $\times g$) at 4°C for 30 min. The supernatants were separated using SDS-PAGE (7%) and blotted onto a polyvinylidene fluoride membrane (pore size, 0.45 μm ; Millipore) by electrotransfer. The membrane was incubated with MAB₁₈₈₆ (10 ng/ml) and then with goat anti-mouse IgG conjugated to HRP (Santa Cruz, Santa Cruz, CA), followed by visualization using an enhanced chemiluminescence (ECL) Western blotting system (Thermo Fisher Scientific, Waltham, MA).

Quantification of eDNA. The isolation of extracellular DNA (eDNA) from the biofilms was performed as described previously (52, 53). Briefly, 24-h-old biofilms cultured in a 96-well polystyrene plate were chilled at 4°C for 1 h, and EDTA was added at a final concentration of 2.5 mM. After measurement of the OD₆₀₀ of the unwashed biofilm (biofilm biomass), eDNA extraction solution (50 mM Tris-HCl, 10 mM EDTA, 500 mM NaCl, pH 8.0) was added to the wells. The biofilms were scraped off and centrifuged (13,000 $\times g$) for 5 min at 4°C. The eDNA in the supernatant was extracted with phenol-chloroform-isoamyl alcohol (25:24:1), precipitated with 100% alcohol, and resuspended in Tris-EDTA buffer. The amount of eDNA was quantified by qPCR with SYBR Premix *Ex Taq* (TaKaRa Bio, Inc., Shiga, Japan) using the primers specific for *gyrB* (gyrase B gene), *serp0306* (ferrichrome transport ATP-binding protein A gene), *leuA* (2-isopropylmalate synthase gene), and *lysA* (diaminopimelate decarboxylase A gene). Each gene was assayed in the qPCR in triplicate in three independent experiments. Relative quantitation of the eDNA in each sample was calculated as the total amount of eDNA (in nanograms) divided by the biofilm biomass (OD₆₀₀).

Measurement of intracellular polyP in the ΔphoU1 and ΔphoU2 mutants. A DAPI (4',6'-diamidino-2-phenylindole)-based fluorescence approach was used to evaluate the amount of intracellular polyP in the *S. epidermidis* cell suspensions as described previously (65). Logarithmic-phase cultures of the *S. epidermidis* strains grown in TSB were collected by centrifugation at 4,000 $\times g$ for 5 min at room temperature. The pellets were washed three times with 100 mM Tris-HCl (pH 7.4) and resuspended in the same buffer to an OD₆₀₀ of 0.2. DAPI (Beyotime) was added to a final concentration of 10 μM . The DAPI fluorescence spectra (excitation, 415 nm; emission, 450 to 650 nm) were recorded using a Cary Eclipse fluorescence spectrophotometer (Varian) after 5 min of agitation at room temperature in the dark. The fluorescence (in arbitrary units) of the DAPI-polyP complex was measured at 550 nm for evaluation of the amount of intracellular polyP.

Detection of intracellular ATP in the ΔphoU1 and ΔphoU2 mutants. The intracellular ATP levels in the ΔphoU1 and ΔphoU2 mutants were detected using an ATP colorimetric/fluorometric assay kit (catalog no. MAK190) from Sigma with modification for *S. epidermidis*. At the time points indicated above and in the relevant figures (when the OD₆₀₀ was 0.5), the cells were pelleted by centrifugation at 4,000 $\times g$ at 4°C, washed with cold sterile PBS, resuspended in 1 ml of ATP extraction buffer within 10 min of initial pelleting of the culture, and lysed with 0.1 mm glass-silica beads in a BeadBeater apparatus (BioSpec). The resulting supernatant, obtained by centrifuging the samples at 20,000 $\times g$ for 15 min at 4°C, was filtered through a 10-kDa-cutoff filter, as suggested by the assay manufacturer, to remove enzymes that could otherwise deplete ATP.

Quantification of intracellular NADP⁺/NADPH in the ΔphoU1 and ΔphoU2 mutants. NADP⁺ and NADPH were quantified as described by Posada et al. using an NADPH/NADP⁺ kit from Sigma, which was modified for *S. epidermidis* (66). Because NADPH can be unstable, the cells were extracted, filtered, and assayed as quickly as possible, essentially as described above.

Sensitivity of the ΔphoU1 and ΔphoU2 mutants to H₂O₂ and SDS. Overnight cultures of the *S. epidermidis* strains were diluted 1:200 in fresh TSB medium and incubated at 37°C for 3 h until an OD₆₀₀ of 1 was reached. After 10-fold serial dilution, 5 μl of the aliquot was spotted onto a TSB agar plate containing 6 mM H₂O₂ or 0.006% SDS and incubated at 37°C overnight. The bacterial colonies on the plates were photographed and counted (5, 31).

MIC and MBC. The MICs of the antibiotics against the five *S. epidermidis* strains were determined using 2-fold serial dilutions of the antibiotics in Mueller-Hinton (MH) broth (Oxoid, Basingstoke, UK) according to CLSI guidelines (67). A log-phase culture (6 h) was adjusted to a turbidity equivalent to that of a 0.5 McFarland standard (10⁸ CFU/ml), inoculated into MH broth (1:200), and then incubated at 37°C for 16 to 20 h. The MIC endpoint was defined as the lowest concentration at which there was no visible growth in the tubes. The broth containing no drugs served as a control. The minimal bactericidal concentration (MBC) values were assessed by plating 100- μl samples from each negative culture tube (tubes with no visible bacterial growth) from the MIC assays onto blank MH broth agar plates. The MBC was the concentration at which a 99.9% reduction of the original inoculum was observed.

Determination of antibiotic-tolerant bacteria. Different antibiotics were added to the stationary-phase cultures (16 h) of the *S. epidermidis* strains (final concentrations, levofloxacin at 50 mg/liter, vancomycin at 75 mg/liter, and amikacin at 50 mg/liter), and then the cultures were incubated at 37°C for 120 h without shaking. One milliliter of the bacterial culture was then washed twice with ice-cold

saline and pelleted by centrifugation for 3 min at $6,000 \times g$, and the pellet was resuspended in 1 ml cold saline, which was used to generate a series of 10-fold dilutions. Triplicate 5- μ l aliquots from each dilution were spotted onto TSA plates for determination of the numbers of CFU (5). Three independent experiments were performed.

RNA isolation and RNA sequencing. Total RNA was isolated from strain SE1457 and the Δ *phoU1* and Δ *phoU2* mutants using an RNeasy minikit (Qiagen, Hilden, Germany) according to the manufacturer's instructions. Briefly, bacterial cultures were centrifuged at $5,000 \times g$ for 5 min, and then the pellets were washed twice in 0.9% saline. The culture was homogenized 5 times using 0.1-mm zirconia-silica beads in a mini-BeadBeater (Biospec, Bartlesville, OK) at 4,800 rpm for 40 s at 1-min intervals on ice. The RNA extracted using the silica-based filter was purified with phenol-chloroform-isoamyl alcohol and precipitated with absolute ethanol.

RNA-Seq was performed according to the Illumina RNA sequencing sample preparation guide, using three biological replicates for each of the *S. epidermidis* strains. Samples of SE1457 and Δ *phoU1* and Δ *phoU2* mutant RNA were treated with RNase-free DNase I (TaKaRa) to prevent contamination with genomic DNA. The RNA quality was evaluated using a Bioanalyzer 2100 system (Agilent Technologies Deutschland GmbH). Prior to the sequencing analysis, rRNA was removed with a RiboZero rRNA removal kit for Gram-positive organisms. After depletion of the rRNA, fragmented RNA was used as a template for PCR with random primers. The cDNA libraries were prepared by using an mRNA-Seq sample preparation kit (Illumina). The concentration of cDNA was measured using a Qubit (version 2.0) fluorometer, the fragment size (200 to 300 bp) was verified on a Bioanalyzer 2100 system, amplification was performed using an Illumina cBot system, and sequencing was performed with an Illumina HiSeq 2500 sequencer for 51 cycles; all of these procedures were performed according to the manufacturers' protocols. Raw sequencing data were processed using the data collection software provided by Illumina.

RNA-Seq data analysis and DEG validation by RT-qPCR. Raw sequencing reads were preprocessed by filtering out rRNA reads, sequencing adapters, short fragment reads, and other low-quality reads. The remaining reads were mapped to the reference genome of *S. epidermidis* RP62A at the NCBI website with Bowtie2 software (version 2.0.5) on the basis of the local alignment algorithm. Reads that aligned to multiple locations were kept (to a maximum of 20 potential positions) to assist with the construction of gene models for genes with repetitive or low-complexity features. When the reads were aligned, 1 mismatch with the reference sequence was allowed. The alignments reported using Bowtie2 software were further processed with BEDTools software to determine the transcript expression levels and their differential expression between each two of the three samples. Expression values were presented as the number of reads per kilobase of genes per million mapped reads (RPKM). Data were visualized using the Integrated Genomics Viewer. Differential expression of all the transcripts was quantified using DEGseq software (version 2.16.1), and then the fold change values were presented. In general, we recorded no distinct difference between two transcripts when their fold change value fell between 0.666 and 1.5. Concomitantly, *P* values were determined, and significance was assessed by correcting for multiple testing using, for example, Fisher's exact test and the Wilcoxon test. Differentially expressed genes with corresponding expression values were uploaded into IPA software and analyzed using the canonical pathway. We used Fisher's exact test to select significant pathways, and the significance threshold was defined by a *P* value of 0.05. The significance of the pathway was indicated by the ratio of the number of genes from the data set that mapped to the pathway versus the total number of genes present in the canonical pathway.

For validation of DEGs identified by RNA-Seq, total RNA extracted from SE1457 and the Δ *phoU1* and Δ *phoU2* mutants was treated with the reagents from a PrimeScript RT reagent kit (TaKaRa Biotechnology, Dalian, China) for DNA digestion and reverse transcribed into cDNA. qPCRs were performed using a Mastercycler RealPlex system (Eppendorf AG, Hamburg, Germany) with SYBR green PCR reagents (SYBR Premix *Ex Taq*; TaKaRa Biotechnology, Dalian, China). The amplification conditions were 95°C for 30 s and 40 cycles of 95°C for 5 s and 60°C for 34 s, followed by a melting curve analysis. *gyrB* (DNA gyrase subunit B gene) was used as a housekeeping gene to normalize the transcript levels of the genes in the qPCR. All RT-qPCRs were performed in triplicate.

Construction of a protein-protein interaction network. A protein-protein interaction network was constructed using Cytoscape software. A total of 174 DEGs encoding the candidate proteins involved in bacterial metabolism were extracted. The protein-protein interaction network was constructed according to the functional relationships annotated in the KEGG database (<http://www.genome.jp/kegg/pathway.html>). In the network, lines were used to represent protein-protein interactions, including binding/association, phosphorylation, activation, and inhibition. Proteins encoded by upregulated and downregulated DEGs are indicated in the figures in red and green, respectively.

Statistical analysis. Experimental data were analyzed with SPSS software and compared using the Student *t* test or one-way analysis of variance. Differences with a *P* value of <0.05 were considered statistically significant.

Accession number(s). The complete RNA-Seq data set is posted in the Gene Expression Omnibus database (<http://www.ncbi.nlm.nih.gov/geo/>) under accession numbers GSE97400 and GSE97656 for the original data set.

SUPPLEMENTAL MATERIAL

Supplemental material for this article may be found at <https://doi.org/10.1128/JB.00219-17>.

SUPPLEMENTAL FILE 1, AVI file, 4.6 MB.

SUPPLEMENTAL FILE 2, AVI file, 4.6 MB.

SUPPLEMENTAL FILE 3, AVI file, 3.4 MB.

SUPPLEMENTAL FILE 4, AVI file, 19.5 MB.

SUPPLEMENTAL FILE 5, AVI file, 16.8 MB.

SUPPLEMENTAL FILE 6, PDF file, 0.7 MB.

ACKNOWLEDGMENTS

We gratefully acknowledge Zonghou Shen (Department of Biochemistry and Molecular Biology, Fudan University) for suggestions on analyzing the DGEs associated with major metabolic pathways.

This work was supported by the National Natural Science Foundation of China (81271791, 81571955, and 81573268) and the National High-Tech and Development Plan of China (2014AA021404).

REFERENCES

- Götz F, Peters G. 2000. Colonization of medical devices by coagulase-negative staphylococci, p 55–88. *In* Waldvogel FA, Bisno AL (ed), *Infections associated with indwelling medical devices*, 3rd ed. American Society for Microbiology, Washington, DC.
- Maduka-Ezeh AN, Greenwood-Quaintance KE, Karau MJ, Barbari EF, Osmon DR, Hanssen AD, Steckelberg JM, Patel R. 2012. Antimicrobial susceptibility and biofilm formation of *Staphylococcus epidermidis* small colony variants associated with prosthetic joint infection. *Diagn Microbiol Infect Dis* 74:224–229. <https://doi.org/10.1016/j.diagmicrobio.2012.06.029>.
- Dunne WM. 2002. Bacterial adhesion: seen any good biofilms lately? *Clin Microbiol Rev* 15:155–166. <https://doi.org/10.1128/CMR.15.2.155-166.2002>.
- Rupp ME, Fey PD, Heilmann C, Gotz F. 2001. Characterization of the importance of *Staphylococcus epidermidis* autolysin and polysaccharide intercellular adhesin in the pathogenesis of intravascular catheter-associated infection in a rat model. *J Infect Dis* 183:1038–1042. <https://doi.org/10.1086/319279>.
- Li Y, Zhang Y. 2007. PhoU is a persistence switch involved in persister formation and tolerance to multiple antibiotics and stresses in *Escherichia coli*. *Antimicrob Agents Chemother* 51:2092–2099. <https://doi.org/10.1128/AAC.00052-07>.
- Shi W, Zhang Y. 2010. PhoY2 but not PhoY1 is the PhoU homologue involved in persisters in *Mycobacterium tuberculosis*. *J Antimicrob Chemother* 65:1237–1242. <https://doi.org/10.1093/jac/dkq103>.
- Wang C, Mao Y, Yu J, Zhu L, Li M, Wang D, Dong D, Liu J, Gao Q. 2013. PhoY2 of mycobacteria is required for metabolic homeostasis and stress response. *J Bacteriol* 195:243–252. <https://doi.org/10.1128/JB.01556-12>.
- de Almeida LG, Ortiz JH, Schneider RP, Spira B. 2015. phoU inactivation in *Pseudomonas aeruginosa* enhances accumulation of ppGpp and polyphosphate. *Appl Environ Microbiol* 81:3006–3015. <https://doi.org/10.1128/AEM.04168-14>.
- Liu J, Lou Y, Yokota H, Adams PD, Kim R, Kim SH. 2005. Crystal structure of a PhoU protein homologue: a new class of metalloprotein containing multinuclear iron clusters. *J Biol Chem* 280:15960–15966. <https://doi.org/10.1074/jbc.M414117200>.
- Chan FY, Torriani A. 1996. PstB protein of the phosphate-specific transport system of *Escherichia coli* is an ATPase. *J Bacteriol* 178:3974–3977. <https://doi.org/10.1128/jb.178.13.3974-3977.1996>.
- Mechler L, Herbig A, Paprotka K, Fraunholz M, Niesel K, Bertram R. 2015. A novel point mutation promotes growth phase-dependent daptomycin tolerance in *Staphylococcus aureus*. *Antimicrob Agents Chemother* 59:5366–5376. <https://doi.org/10.1128/AAC.00643-15>.
- Mechler L, Bonetti EJ, Reichert S, Flotenmeyer M, Schrenzel J, Bertram R, Francois P, Gotz F. 2016. Daptomycin tolerance in the *Staphylococcus aureus* pitA6 mutant is due to upregulation of the *dlt* operon. *Antimicrob Agents Chemother* 60:2684–2691. <https://doi.org/10.1128/AAC.03022-15>.
- Lewis K. 2007. Persister cells, dormancy and infectious disease. *Nat Rev Microbiol* 5:48–56. <https://doi.org/10.1038/nrmicro1557>.
- Otto M. 2008. Staphylococcal biofilms. *Curr Top Microbiol Immunol* 322:207–228.
- Winkler ME, Hoch JA. 2008. Essentiality, bypass, and targeting of the YycFG (VicRK) two-component regulatory system in gram-positive bacteria. *J Bacteriol* 190:2645–2648. <https://doi.org/10.1128/JB.01682-07>.
- Masalha M, Borovok I, Schreiber R, Aharonowitz Y, Cohen G. 2001. Analysis of transcription of the *Staphylococcus aureus* aerobic class Ib and anaerobic class III ribonucleotide reductase genes in response to oxygen. *J Bacteriol* 183:7260–7272. <https://doi.org/10.1128/JB.183.24.7260-7272.2001>.
- Fuchs S, Pane-Farre J, Kohler C, Hecker M, Engelmann S. 2007. Anaerobic gene expression in *Staphylococcus aureus*. *J Bacteriol* 189:4275–4289. <https://doi.org/10.1128/JB.00081-07>.
- Leibig M, Liebeke M, Mader D, Lalk M, Peschel A, Gotz F. 2011. Pyruvate formate lyase acts as a formate supplier for metabolic processes during anaerobiosis in *Staphylococcus aureus*. *J Bacteriol* 193:952–962. <https://doi.org/10.1128/JB.01161-10>.
- Wu Y, Wu Y, Zhu T, Han H, Liu H, Xu T, Francois P, Fischer A, Bai L, Gotz F, Qu D. 2015. *Staphylococcus epidermidis* SrrAB regulates bacterial growth and biofilm formation differently under oxic and microaerobic conditions. *J Bacteriol* 197:459–476. <https://doi.org/10.1128/JB.02231-14>.
- Kazmierczak MJ, Wiedmann M, Boor KJ. 2005. Alternative sigma factors and their roles in bacterial virulence. *Microbiol Mol Biol Rev* 69:527–543. <https://doi.org/10.1128/MMBR.69.4.527-543.2005>.
- Heilmann C, Hussain M, Peters G, Gotz F. 1997. Evidence for autolysin-mediated primary attachment of *Staphylococcus epidermidis* to a polystyrene surface. *Mol Microbiol* 24:1013–1024. <https://doi.org/10.1046/j.1365-2958.1997.4101774.x>.
- Lang S, Xu J, Stuart F, Thomas RM, Vrijbloed JW, Robinson JA. 2000. Analysis of antibody A6 binding to the extracellular interferon gamma receptor alpha-chain by alanine-scanning mutagenesis and random mutagenesis with phage display. *Biochemistry* 39:15674–15685. <https://doi.org/10.1021/bi000838z>.
- Buist G, Steen A, Kok J, Kuipers OP. 2008. LysM, a widely distributed protein motif for binding to (peptidoglycan)s. *Mol Microbiol* 68:838–847. <https://doi.org/10.1111/j.1365-2958.2008.06211.x>.
- Hensley K, Robinson KA, Gabbita SP, Salsman S, Floyd RA. 2000. Reactive oxygen species, cell signaling, and cell injury. *Free Radic Biol Med* 28:1456–1462. [https://doi.org/10.1016/S0891-5849\(00\)00252-5](https://doi.org/10.1016/S0891-5849(00)00252-5).
- Nordberg J, Arner ES. 2001. Reactive oxygen species, antioxidants, and the mammalian thioredoxin system. *Free Radic Biol Med* 31:1287–1312. [https://doi.org/10.1016/S0891-5849\(01\)00724-9](https://doi.org/10.1016/S0891-5849(01)00724-9).
- Lee SM, Koh HJ, Park DC, Song BJ, Huh TL, Park JW. 2002. Cytosolic NADP(+)-dependent isocitrate dehydrogenase status modulates oxidative damage to cells. *Free Radic Biol Med* 32:1185–1196. [https://doi.org/10.1016/S0891-5849\(02\)00815-8](https://doi.org/10.1016/S0891-5849(02)00815-8).
- Maeng O, Kim YC, Shin HJ, Lee JO, Huh TL, Kang KI, Kim YS, Paik SG, Lee H. 2004. Cytosolic NADP(+)-dependent isocitrate dehydrogenase protects macrophages from LPS-induced nitric oxide and reactive oxygen species. *Biochem Biophys Res Commun* 317:558–564. <https://doi.org/10.1016/j.bbrc.2004.03.075>.
- Giro M, Carrillo N, Krapp AR. 2006. Glucose-6-phosphate dehydrogenase and ferredoxin-NADP(H) reductase contribute to damage repair during

- the soxRS response of *Escherichia coli*. *Microbiology* 152:1119–1128. <https://doi.org/10.1099/mic.0.28612-0>.
29. Marino D, Gonzalez EM, Frendo P, Puppo A, Arrese-Igor C. 2007. NADPH recycling systems in oxidative stressed pea nodules: a key role for the NADP⁺-dependent isocitrate dehydrogenase. *Planta* 225:413–421.
 30. Kornberg A. 1999. Inorganic polyphosphate: a molecule of many functions. *Prog Mol Subcell Biol* 23:1–18. https://doi.org/10.1007/978-3-642-58444-2_1.
 31. Liu X, Sun X, Wu Y, Xie C, Zhang W, Wang D, Chen X, Qu D, Gan J, Chen H, Jiang H, Lan L, Yang CG. 2013. Oxidation-sensing regulator AbfR regulates oxidative stress responses, bacterial aggregation, and biofilm formation in *Staphylococcus epidermidis*. *J Biol Chem* 288:3739–3752. <https://doi.org/10.1074/jbc.M112.426205>.
 32. Surin BP, Rosenberg H, Cox GB. 1985. Phosphate-specific transport system of *Escherichia coli*: nucleotide sequence and gene-polypeptide relationships. *J Bacteriol* 161:189–198.
 33. Kim SK, Makino K, Amemura M, Shinagawa H, Nakata A. 1993. Molecular analysis of the phoH gene, belonging to the phosphate regulon in *Escherichia coli*. *J Bacteriol* 175:1316–1324. <https://doi.org/10.1128/jb.175.5.1316-1324.1993>.
 34. Morohoshi T, Maruo T, Shirai Y, Kato J, Ikeda T, Takiguchi N, Ohtake H, Kuroda A. 2002. Accumulation of inorganic polyphosphate in phoU mutants of *Escherichia coli* and *Synechocystis* sp. strain PCC6803. *Appl Environ Microbiol* 68:4107–4110. <https://doi.org/10.1128/AEM.68.8.4107-4110.2002>.
 35. Beard SJ, Hashim R, Wu G, Binet MR, Hughes MN, Poole RK. 2000. Evidence for the transport of zinc(II) ions via the pit inorganic phosphate transport system in *Escherichia coli*. *FEMS Microbiol Lett* 184:231–235. <https://doi.org/10.1111/j.1574-6968.2000.tb09019.x>.
 36. Vershinina OA, Znamenskaya LV. 2002. The Pho regulons of bacteria. *Mikrobiologiya* 71:581–595. (In Russian.)
 37. Steed PM, Wanner BL. 1993. Use of the *rep* technique for allele replacement to construct mutants with deletions of the *pstSCAB-phoU* operon: evidence of a new role for the PhoU protein in the phosphate regulon. *J Bacteriol* 175:6797–6809. <https://doi.org/10.1128/jb.175.21.6797-6809.1993>.
 38. Sun G, Sharkova E, Chesnut R, Birkey S, Duggan MF, Sorokin A, Pujic P, Ehrlich SD, Hulett FM. 1996. Regulators of aerobic and anaerobic respiration in *Bacillus subtilis*. *J Bacteriol* 178:1374–1385. <https://doi.org/10.1128/jb.178.5.1374-1385.1996>.
 39. Roca I, Torrents E, Sahlin M, Gibert I, Sjöberg BM. 2008. NrdI essentiality for class Ib ribonucleotide reduction in *Streptococcus pyogenes*. *J Bacteriol* 190:4849–4858. <https://doi.org/10.1128/JB.00185-08>.
 40. Kinkel TL, Roux CM, Dunman PM, Fang FC. 2013. The *Staphylococcus aureus* SrrAB two-component system promotes resistance to nitrosative stress and hypoxia. *mBio* 4:e00696-13. <https://doi.org/10.1128/mBio.00696-13>.
 41. Fabret C, Hoch JA. 1998. A two-component signal transduction system essential for growth of *Bacillus subtilis*: implications for anti-infective therapy. *J Bacteriol* 180:6375–6383.
 42. Dubrac S, Bisicchia P, Devine KM, Msadek T. 2008. A matter of life and death: cell wall homeostasis and the WalKR (YycGF) essential signal transduction pathway. *Mol Microbiol* 70:1307–1322. <https://doi.org/10.1111/j.1365-2958.2008.06483.x>.
 43. Chai Y, Beauregard PB, Vlamakis H, Losick R, Kolter R. 2012. Galactose metabolism plays a crucial role in biofilm formation by *Bacillus subtilis*. *mBio* 3:e00184-12. <https://doi.org/10.1128/mBio.00184-12>.
 44. Bera A, Biswas R, Herbert S, Kulazovic E, Weidenmaier C, Peschel A, Gotz F. 2007. Influence of wall teichoic acid on lysozyme resistance in *Staphylococcus aureus*. *J Bacteriol* 189:280–283. <https://doi.org/10.1128/JB.01221-06>.
 45. Schlag M, Biswas R, Krismer B, Kohler T, Zoll S, Yu W, Schwarz H, Peschel A, Gotz F. 2010. Role of staphylococcal wall teichoic acid in targeting the major autolysin Atl. *Mol Microbiol* 75:864–873. <https://doi.org/10.1111/j.1365-2958.2009.07007.x>.
 46. Andrey DO, Renzoni A, Monod A, Lew DP, Cheung AL, Kelley WL. 2010. Control of the *Staphylococcus aureus* toxic shock *tst* promoter by the global regulator SarA. *J Bacteriol* 192:6077–6085. <https://doi.org/10.1128/JB.00146-10>.
 47. Rao NN, Gomez-Garcia MR, Kornberg A. 2009. Inorganic polyphosphate: essential for growth and survival. *Annu Rev Biochem* 78:605–647. <https://doi.org/10.1146/annurev.biochem.77.083007.093039>.
 48. Davidson AL, Dassa E, Orelle C, Chen J. 2008. Structure, function, and evolution of bacterial ATP-binding cassette systems. *Microbiol Mol Biol Rev* 72:317–364. <https://doi.org/10.1128/MMBR.00031-07>.
 49. Conlon BP, Rowe SE, Gandt AB, Nuxoll AS, Donegan NP, Zalis EA, Clair G, Adkins JN, Cheung AL, Lewis K. 2016. Persister formation in *Staphylococcus aureus* is associated with ATP depletion. *Nat Microbiol* 1:16051. <https://doi.org/10.1038/nmicrobiol.2016.51>.
 50. Gill SR, Fouts DE, Archer GL, Mongodin EF, Deboy RT, Ravel J, Paulsen IT, Kolonay JF, Brinkac L, Beanan M, Dodson RJ, Daugherty SC, Madupu R, Angiuoli SV, Durkin AS, Haft DH, Vamathevan J, Khouri H, Utterback T, Lee C, Dimitrov G, Jiang L, Qin H, Weidman J, Tran K, Kang K, Hance IR, Nelson KE, Fraser CM. 2005. Insights on evolution of virulence and resistance from the complete genome analysis of an early methicillin-resistant *Staphylococcus aureus* strain and a biofilm-producing methicillin-resistant *Staphylococcus epidermidis* strain. *J Bacteriol* 187:2426–2438. <https://doi.org/10.1128/JB.187.7.2426-2438.2005>.
 51. Bae T, Schneewind O. 2006. Allelic replacement in *Staphylococcus aureus* with inducible counter-selection. *Plasmid* 55:58–63. <https://doi.org/10.1016/j.plasmid.2005.05.005>.
 52. Zhu T, Lou Q, Wu Y, Hu J, Yu F, Qu D. 2010. Impact of the *Staphylococcus epidermidis* LytSR two-component regulatory system on murein hydrolase activity, pyruvate utilization and global transcriptional profile. *BMC Microbiol* 10:287. <https://doi.org/10.1186/1471-2180-10-287>.
 53. Lou Q, Zhu T, Hu J, Ben H, Yang J, Yu F, Liu J, Wu Y, Fischer A, Francois P, Schrenzel J, Qu D. 2011. Role of the SaeRS two-component regulatory system in *Staphylococcus epidermidis* autolysis and biofilm formation. *BMC Microbiol* 11:146. <https://doi.org/10.1186/1471-2180-11-146>.
 54. Helle L, Kull M, Mayer S, Marincola G, Zelder ME, Goerke C, Wolz C, Bertram R. 2011. Vectors for improved Tet repressor-dependent gradual gene induction or silencing in *Staphylococcus aureus*. *Microbiology* 157:3314–3323. <https://doi.org/10.1099/mic.0.052548-0>.
 55. Charpentier E, Anton AI, Barry P, Alfonso B, Fang Y, Novick RP. 2004. Novel cassette-based shuttle vector system for gram-positive bacteria. *Appl Environ Microbiol* 70:6076–6085. <https://doi.org/10.1128/AEM.70.10.6076-6085.2004>.
 56. Gust AA, Biswas R, Lenz HD, Rauhut T, Ranf S, Kemmerling B, Gotz F, Glawischnig E, Lee J, Felix G, Nurnberger T. 2007. Bacteria-derived peptidoglycans constitute pathogen-associated molecular patterns triggering innate immunity in Arabidopsis. *J Biol Chem* 282:32338–32348. <https://doi.org/10.1074/jbc.M704886200>.
 57. Vollmer W, Seligman SJ. 2010. Architecture of peptidoglycan: more data and more models. *Trends Microbiol* 18:59–66. <https://doi.org/10.1016/j.tim.2009.12.004>.
 58. Christensen GD, Simpson WA, Younger JJ, Baddour LM, Barrett FF, Melton DM, Beachey EH. 1985. Adherence of coagulase-negative staphylococci to plastic tissue culture plates: a quantitative model for the adherence of staphylococci to medical devices. *J Clin Microbiol* 22:996–1006.
 59. Qin Z, Ou Y, Yang L, Zhu Y, Tolker-Nielsen T, Molin S, Qu D. 2007. Role of autolysin-mediated DNA release in biofilm formation of *Staphylococcus epidermidis*. *Microbiology* 153:2083–2092. <https://doi.org/10.1099/mic.0.2007/006031-0>.
 60. Hu J, Xu T, Zhu T, Lou Q, Wang X, Wu Y, Huang R, Liu J, Liu H, Yu F, Ding B, Huang Y, Tong W, Qu D. 2011. Monoclonal antibodies against accumulation-associated protein affect EPS biosynthesis and enhance bacterial accumulation of *Staphylococcus epidermidis*. *PLoS One* 6:e20918. <https://doi.org/10.1371/journal.pone.0020918>.
 61. Lam H, Kesselly A, Stegalkina S, Charlebois RL, Oomen R, Kleanthous H, Yethon JA. 2015. Correction for Lam et al., antibodies to PhnD inhibit staphylococcal biofilms. *Infect Immun* 83:2197. <https://doi.org/10.1128/IAI.00285-15>.
 62. Brunskill EW, Bayles KW. 1996. Identification and molecular characterization of a putative regulatory locus that affects autolysis in *Staphylococcus aureus*. *J Bacteriol* 178:611–618. <https://doi.org/10.1128/jb.178.3.611-618.1996>.
 63. Gerke C, Kraft A, Sussmuth R, Schweitzer O, Gotz F. 1998. Characterization of the N-acetylglucosaminyltransferase activity involved in the biosynthesis of the *Staphylococcus epidermidis* polysaccharide intercellular adhesin. *J Biol Chem* 273:18586–18593. <https://doi.org/10.1074/jbc.273.29.18586>.
 64. Wu Y, Wang J, Xu T, Liu J, Yu W, Lou Q, Zhu T, He N, Ben H, Hu J, Gotz F, Qu D. 2012. The two-component signal transduction system ArlRS regulates *Staphylococcus epidermidis* biofilm formation in an ica-dependent manner. *PLoS One* 7:e40041. <https://doi.org/10.1371/journal.pone.0040041>.

65. Aschar-Sobbi R, Abramov AY, Diao C, Kargacin ME, Kargacin GJ, French RJ, Pavlov E. 2008. High sensitivity, quantitative measurements of polyphosphate using a new DAPI-based approach. *J Fluoresc* 18: 859–866. <https://doi.org/10.1007/s10895-008-0315-4>.
66. Posada AC, Kolar SL, Dusi RG, Francois P, Roberts AA, Hamilton CJ, Liu GY, Cheung A. 2014. Importance of bacillithiol in the oxidative stress response of *Staphylococcus aureus*. *Infect Immun* 82:316–332. <https://doi.org/10.1128/IAI.01074-13>.
67. Turnidge J, Bordash G. 2007. Statistical methods for establishing quality control ranges for antibacterial agents in Clinical and Laboratory Standards Institute susceptibility testing. *Antimicrob Agents Chemother* 51: 2483–2488. <https://doi.org/10.1128/AAC.01457-06>.